

Article

3D-Printing of Capsule Devices as Compartmentalization Tools for Supported Reagents in the Search of Antiproliferative Isatins

Camilla Malatini ¹, Carlos Carbajales ¹ , Mariángel Luna ², Osvaldo Beltrán ², Manuel Amorín ¹, Christian F. Masaguer ¹ , José M. Blanco ¹, Silvia Barbosa ² , Pablo Taboada ^{2,*}  and Alberto Coelho ^{1,*}

¹ Departamento de Química Orgánica, Facultad de Farmacia, Universidade de Santiago de Compostela, 15782 Santiago de Compostela, Spain

² Departamento de Física de la Materia Condensada, Facultad de Física, Universidad de Santiago de Compostela, CP 15782 Santiago de Compostela, Spain

* Correspondence: pablo.taboada@usc.es (P.T.); albertojoose.coelho@usc.es (A.C.)

Abstract: The application of high throughput synthesis methodologies in the generation of active pharmaceutical ingredients (APIs) currently requires the use of automated and easily scalable systems, easy dispensing of supported reagents in solution phase organic synthesis (SPOS), and elimination of purification and extraction steps. The recyclability and recoverability of supported reagents and/or catalysts in a rapid and individualized manner is a challenge in the pharmaceutical industry. This objective can be achieved through a suitable compartmentalization of these pulverulent reagents in suitable devices for it. This work deals with the use of customized polypropylene permeable-capsule devices manufactured by 3D printing, using the fused deposition modeling (FDM) technique, adaptable to any type of flask or reactor. The capsules fabricated in this work were easily loaded “in one step” with polymeric reagents for use as scavengers of isocyanides in the work-up process of Ugi multicomponent reactions or as compartmentalized and reusable catalysts in copper-catalyzed cycloadditions (CuAAC) or Heck palladium catalyzed cross-coupling reactions (PCCCRs). The reaction products are different series of diversely substituted isatins, which were tested in cancerous cervical HeLa and murine 3T3 Balb fibroblast cells, obtaining potent antiproliferative activity. This work demonstrates the applicability of 3D printing in chemical processes to obtain anticancer APIs.

Keywords: 3D printing; catalyst compartmentation; polypropylene capsule; supported reagents; isatins; anticancer



Citation: Malatini, C.; Carbajales, C.; Luna, M.; Beltrán, O.; Amorín, M.; Masaguer, C.F.; Blanco, J.M.; Barbosa, S.; Taboada, P.; Coelho, A.

3D-Printing of Capsule Devices as Compartmentalization Tools for Supported Reagents in the Search of Antiproliferative Isatins.

Pharmaceuticals **2023**, *16*, 310.

<https://doi.org/10.3390/ph16020310>

Academic Editor: Touraj Ehtezazi

Received: 31 December 2022

Revised: 27 January 2023

Accepted: 9 February 2023

Published: 16 February 2023



Copyright: © 2023 by the authors. Licensee MDPI, Basel, Switzerland. This article is an open access article distributed under the terms and conditions of the Creative Commons Attribution (CC BY) license (<https://creativecommons.org/licenses/by/4.0/>).

1. Introduction

Three-dimensional printing is a revolutionary technology in many scientific fields today. Some of its scopes have a great impact on health sciences and particularly on medicine [1,2]. The application of 3D printing in the field of chemistry in general and specifically in pharmaceutical chemistry has been driven mainly by the initial work of Cronin and collaborators [3,4] through the design of polypropylene reactors with different shapes and compartments that make the concept of automated synthesis of “drugs on demand” a reality [5]. These initial works highlighted concepts of extraordinary importance today, such as easy work up or to facilitate the dispensing of reagents by automated robotic systems connected to multimedia systems. Collectively, behind these studies is the idea of “democratizing” and digitizing the syntheses and their scale up in many laboratories [6]. This goal is even more feasible if we consider the considerable technological advancement of 3D printers in recent years [7,8]. On the other hand, there is currently an increasingly deep concern for the development of recyclable and/or reusable materials and devices and, particularly in the field of green chemistry, regarding the development of heterogeneous catalysts or effective polymeric reagents [9]. Good examples of this class of reagents are

polymeric ones containing gold, palladium, platinum, ruthenium, or copper metal and even scavenger-type polymers for toxic substances, among others [10–14]. Particularly powerful are the copper-catalyzed alkyne-azide cycloadditions (CuAAC, the flagship of the click chemistry) or the palladium-catalyzed cross-coupling reactions (PCCCRs) [15–17]. However, many of the heterogeneous catalysts have a very small particle size (in general, metal nanoparticles [18], silicas [19], and mainly polystyrene-based polymers [20]). In the case of polymeric reagents, the size range is highly variable, but many are found in diameters of a few hundred microns thick. This implies that the solid reagent or heterogeneous catalyst, which in many cases is expensive, must be separated from the reaction medium by filtration to be recycled or reused. In many cases, it would be interesting to be able to use two solid catalysts simultaneously (for use in tandem processes [21], cooperative bimetallic catalysis [22,23], multicatalytic one-pot procedures [24], etc.) enabling their reuse separately. Therefore, from a practical point of view, the compartmentalization of catalysts is an interesting objective in the coming years.

The concept of catalyst compartmentalization [25,26] was promoted by Houghten in the 80s, mainly through the “tea bag technique” [27] and was applied to combinatorial chemistry. Another impulse in this sense was contributed by Jones and other groups, using magnetic nanoparticles, easily extractable from the reaction medium and allowing consecutive “one pot” functionalizations with incompatible reagents, such as acids and bases [28–30]. In any case, the use of solid materials in solution phase organic synthesis (SPOS) depends on their adaptability and chemical resistance to the reaction mixture, so the selection of the material is very important. Our research group has carried out multi-component heterogeneous multicatalytic syntheses (MCRs) including 3D-printed ceramic monoliths in the reaction cocktails [31], in which two compartmentalized catalysts in each monolith can carry out these kinds of transformations. A crucial aspect in these procedures is that the metal species remains immobilized on the support or heterogeneous catalytic material, allowing its reuse and, at the same time, avoiding the contamination of the reaction medium with the metallic species and, therefore, the drug. This aspect is fundamental if we consider the strict controls imposed by international agencies for evaluation of medicinal products regarding the presence of these metals in the final drugs [32].

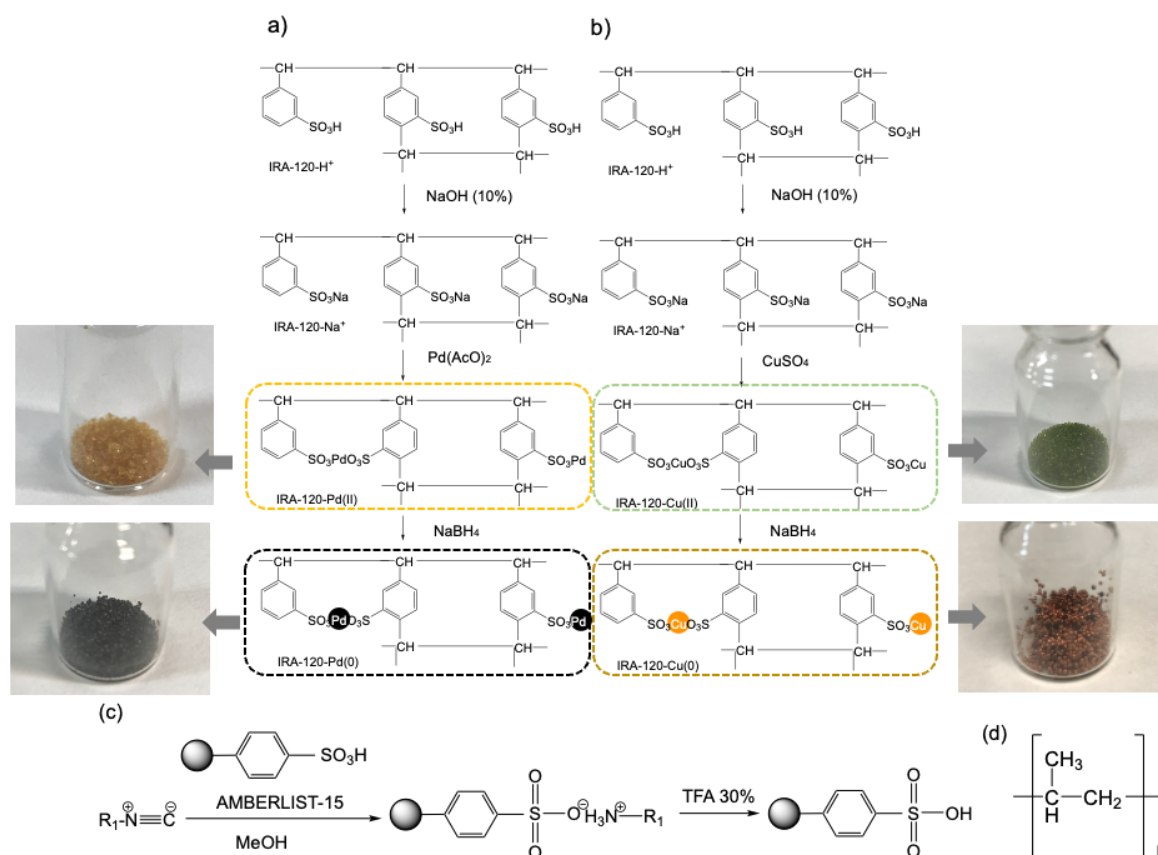
The isatin (1H-indole-2,3-dione) nucleus is a privileged scaffold in medicinal chemistry. The versatility of isatin’s molecular architecture makes it an ideal scaffold for structural modification and functionalization as evidenced by the fact that many isatin derivatives exhibit a broad range of biological activities [33–39]. Particularly comprehensive are the reviews by the groups of Shankaraiah and Costa Ferreira about the anti-neoplastic activity of variously substituted isatins [40,41]. Among the structural modifications carried out on the scaffold for the search of new antitumoral chemodrugs, those carried out on position 3 of the oxindole stand out, either through the formation of 3-imino, 3-hydrazine-ylidene, and especially 3-alkylideneindolin-2-one type bonds or through the development of Ugi-type multicomponent reactions (MCRs) [42]. This has given rise to very powerful and effective drugs such as the experimental drug Orantinib [43,44], the commercialized Sunitinib [45] or Nintedanib [46]. The transformations also were jointly carried out in positions 1 and 5, which have given rise to compounds with potent anti-neoplastic activity [47–50].

Here, we present an integrated work including drug synthesis, 3D printing of materials, and biological evaluation of bioactive compounds. Three series of isatin-type biomolecules are presented using supported reagents, either acting as catalysts in CuAAC or Heck reactions [51] as well as isocyanide scavengers (reagents with a very unpleasant odor) in Ugi-type MCRs [52]. The supported reagents are compartmentalized in novel reusable custom porous capsule-type structures, in polypropylene material, using 3D-printing technology. The use of these capsules favors both the dispensing and handling of supported reagents as well as the work up, avoiding filtration stages and recovering the precious reagent for reuse. In addition, we present the preliminary results of the antiproliferative activity of these small series of prepared molecules in tumor cell lines.

2. Results and Discussion

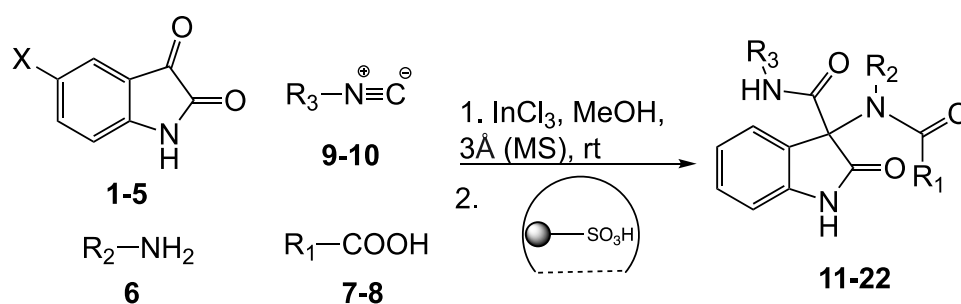
The workflow in this study can be summarized in the following points:

- Preparation of the catalytic systems to be compartmentalized (Scheme 1). Synthesis of efficient and robust resin–metal heterogeneous catalysts IRA-120-Cu and IRA-120-Pd (Section 2.1).
- Computer-aided design of novel capsule prototypes using the editing programs Tinkercad[®] and Cura[®] (Section 2.2).
- Manufacture of PP capsule prototypes using 3D printing (fused deposition modeling) with a semipermeable membrane, enabling the compartmentation of the metal–resin type catalysts of the first point, providing Capsule@IRA-120-Cu(0) and Capsule@IRA-120-Pd(0). In addition, enabling the compartmentation of the isocyanide scavenger Amberlyst-15 to create Capsule@Amberlyst-15 [53]. This supported reagent is a brown-gray granule reticular polystyrene based on ion exchange resins with strong acidic sulfonic groups (Scheme 1c). It is used as a strongly acidic heterogeneous acid catalysis and is suitable for nonaqueous catalysis.
- Study of the chemical stability of the capsule as a resin container, according to the reaction conditions (solvent, base, and temperature), to carry out the CuAAC or Heck reactions as well as the scavenging of isocyanide in Ugi reactions. (Section 2.2).
- Study of the behavior of the capsule–catalyst pairing. Application to heterogeneous catalysis as CuAAC reactions or PCCCRs (Heck) or as isocyanide scavenger (Ugi). Study of the recyclability of the resins and the capsules. Customization of capsule designs (of different sizes), aiming to carry out reactions at different scales (from milligrams to grams) (Sections 2.3 and 2.4).



Scheme 1. (a) Synthesis of IRA-120-Pd(0) for Heck reactions and (b) IRA-120-Cu(0) catalyst for CuAAC. (c) Chemical scavenging of isocyanides by Amberlyst-15 and recycling process in TFA. (d) Structure of the PP monomer.

The first efforts were aimed at optimizing appropriate reaction conditions for each isatin series (Schemes 2 and 3). Series 1 corresponding to the Ugi reactions (Scheme 1) was carried out using a classical procedure, (see Section 2.3) following the methodology of Pineiro et al. but using the Amberlyst-15 resin as a scavenger of excess isocyanide in the work-up process, after the Ugi reactions. The intense and repulsive odor of the isocyanide compounds was described as overpowering and extremely distressing by Hofmann and Gautier [54,55], discouraging many potential contributors to this field. Isocyanides can be extremely unpleasant in odor and toxicity (cyclohexyl isocyanide), which also depends on their degree of volatility. Therefore, the use of scavengers facilitates safe work in the laboratory. The use of PS-TsOH-type resins as an effective isocyanide scavenger was previously reported by our group [56,57]. Series 2 corresponds to three examples of CuAAC to generate triazole-type structures at position 1 of isatin. Series 3 corresponds to examples of Heck-type PCCCRs reactions to generate bioactive structures that have alkenyl functions in position 5 or benzylic substituents in position 1. For the synthesis of series 2 and 3, supported catalysts containing copper or palladium (0) nanoparticles were prepared, respectively.

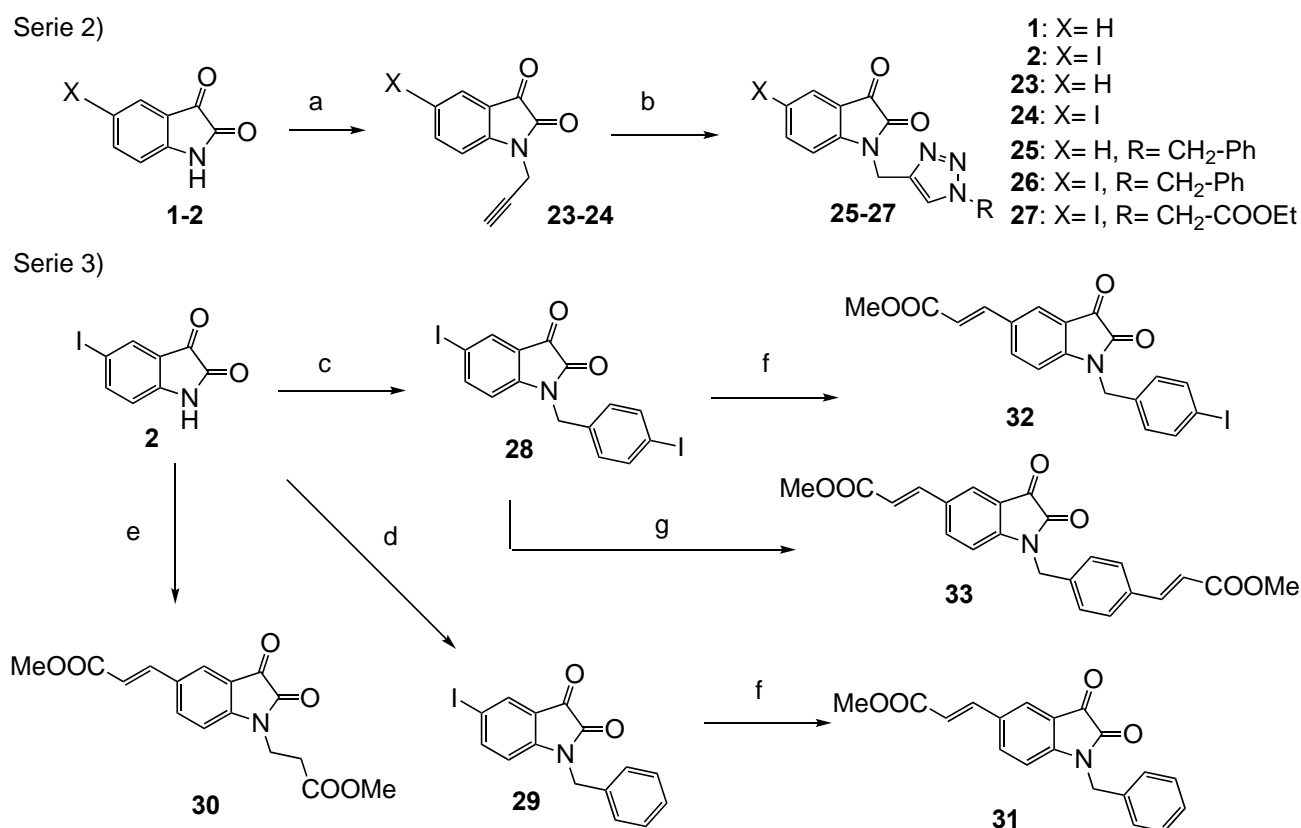


Scheme 2. General conditions for Ugi: isatin derivative 1–5 (200 mg, 1 equiv), InCl_3 (10 mol%), 150 mg of MS 3 Å and methanol (1 mL), *n*-butylamine (1.5 equiv), isocyanide (1.5 equiv), and carboxylic acid (1.5 equiv), rt.

2.1. Synthesis of the Catalytic Materials IRA-120-Cu(0) and IRA-120-Pd(0)

The preparation of the catalytic materials necessary to carry out the syntheses of series 2 and 3, was carried out in a similar way to that described by Silva and coworkers, starting from acidic ion exchange polystyrene resin IRA-120-H [58,59]. The procedure pursued a surface exchange of H^+ ions for Na^+ ions after treatment of the IRA-120H resin with NaOH (10%) overnight (Scheme 1). Once the new IRA-120Na resin was obtained, it was treated with the appropriate salt (CuSO_4 in water or $\text{Pd}(\text{AcO})_2$ in acetone/water) to provide both IRA-120-Cu(II) (green color) and IRA-120-Pd(II) (light brown color) intermediate catalytic materials. A final treatment with NaBH_4 provided the final resins loaded with copper or palladium nanoparticles, IRA-120-Cu(0) or IRA-120-Pd(0). The final treatment of the intermediate resins produces a drastic change in the color of the resin as a consequence of the change in the oxidation state. The metal nanoparticles (Pd or Cu) remain immobilized in the polyionic environment.

Catalytic resins loaded with copper or palladium species were analyzed by FESEM and EDX experiments. The distribution of both palladium and copper on the 3D-printed spherical bead surfaces were experimentally confirmed. Nanoparticles were found both within the resin and on the surface. The EDX analysis of the samples showed that the loading levels of both species were similar, 21.7% [IRA-Cu(0)] and 22.29% [IRA-Pd(0)]. As can be seen in Figure 1, the dispersion of the metal is more uniform along the surface of IRA-Cu(0) than in IRA-Pd(0).



Scheme 3. (a) K₂CO₃ anh., propargyl bromide, MeCN, 50 °C. (b) Capsule@IRA-120-Cu(0), alkyne, R-N₃, MeCN, 10 h. (c) K₂CO₃ anh., 4-iodo-benzyl bromide, MeCN, 50 °C, 12 h. (d) K₂CO₃ anh., benzyl bromide, MeCN, 70 °C. (e) Capsule@IRA-120-Pd(0), methyl acrylate (exc), 90 °C, sodium acetate, DMF/H₂O, 24 h. (f) Capsule@IRA-120-Pd(0), methyl acrylate, sodium acetate, 70 °C, DMF/H₂O, 24 h. (g) Capsule@IRA-120-Pd(0), methyl acrylate (exc), sodium acetate, 90 °C, DMF/H₂O, 12 h.

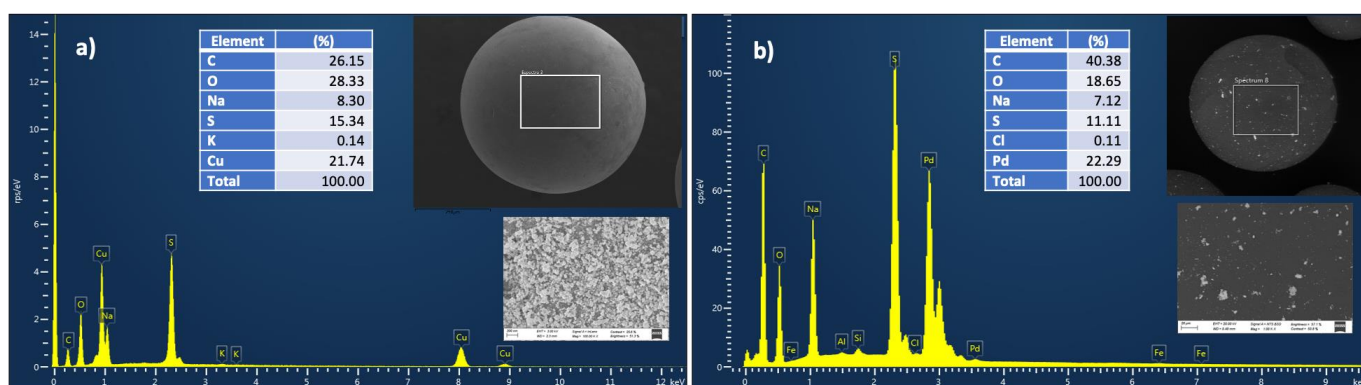


Figure 1. (a) EDX and FESEM of IRA-120-Cu(0) catalyst for CuAAC. (b) IRA-120-Pd(0) for Heck reactions (see graphics in detail in supplementary material Figure S2).

2.2. Fabrication of the Polypropylene Capsules and Compartmentation of Amberlyst 15 and the Catalytic Materials IRA-120-Cu(0) and IRA-120-Pd(0)

We present, here, an innovative, cost effective, simple, and practical porous capsule manufacture for the entrapment of the supported reagents Amberlite-IRA-120-Cu(0) and Amberlite-IRA-120-Pd(0) described in the previous section as well as the commercial Amberlyst-15, to produce Capsule@IRA-120-Cu(0), Capsule@IRA-120-Pd(0), and Capsule@Amberlyst-15, respectively.

2.2.1. Computer-Aided Design (CAD)

These capsules were designed by CAD and synthesized using 3D printing with the aim of miniaturizing and minimizing the work-up operations. The 3D design was performed using the Tinkercad[®] and Cura[®] programs. The capsule design itself was thought to be able to carry out the printing and loading processes of the polymeric material in a single stage (see Section 3). After evaluating the possible unicompartimental designs (Figure 2a,e,f,k), a capsule with a bicompartimental design was chosen (Figure 2b,g,j). With this last new design, there is the possibility of introducing a magnetic stirrer into one of the interior compartments and, into the other, the desired resin. Thus, as can be seen in Figure 2, by incorporating a magnetic stirrer inside the capsule, in a different compartment, the resin is not damaged by direct mechanical stress due to contact with the magnetic stirrer. At the same time, it provides the capsule with autonomous movement and flow is very favorable for the exchange of reagents within it. This exchange is favored by certain solvents (by swelling) or by a slight increase in temperature, favoring pore opening of the semipermeable membrane and, therefore, the entry and exit of reactants and products. In any case, the solid catalyst remains inside the capsule during the process. The ultimate aim of these devices is to offer an alternative to the handling of polymeric reagents without the need for orbital stirring devices.

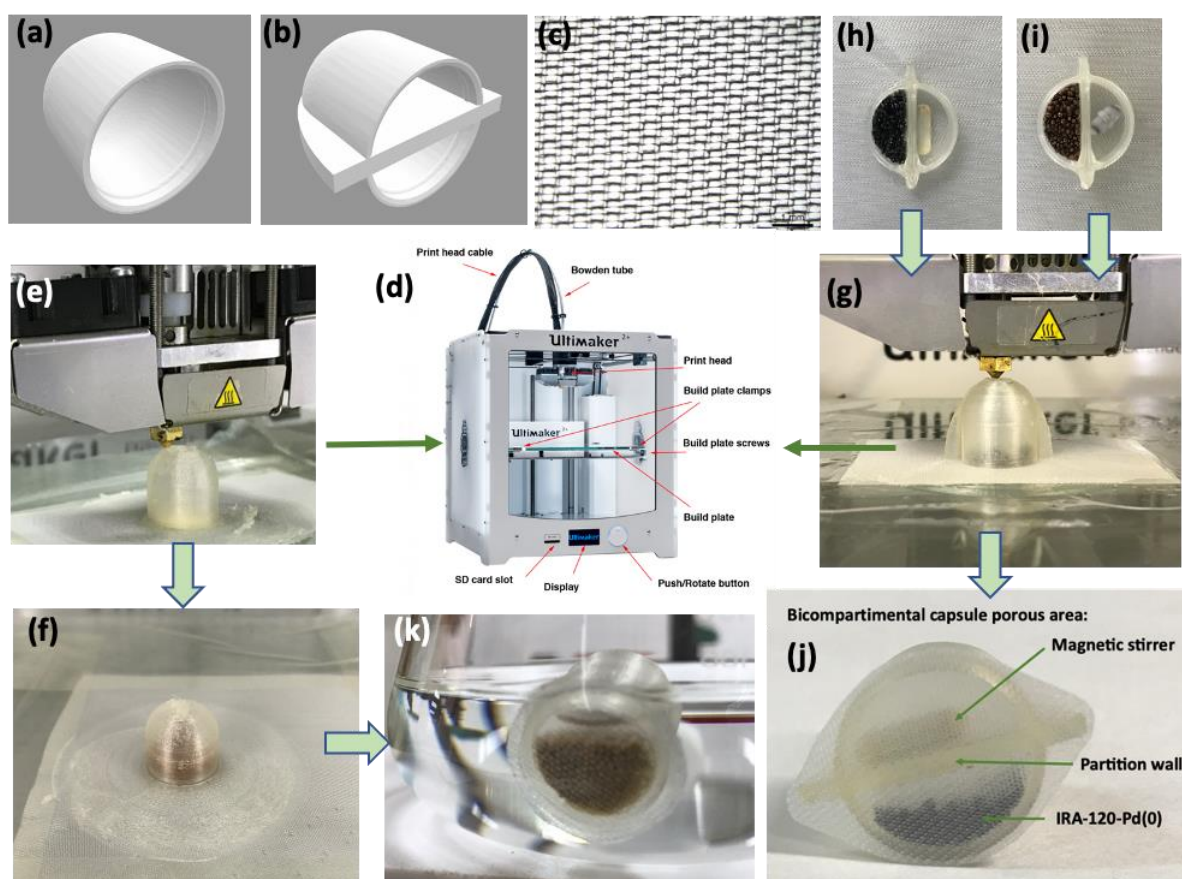


Figure 2. (a) The 3D design of a unicompartimental capsule (see also Figure S1); (b) bicompartimental capsule; (c) polypropylene mesh (bar scale 1 mm); (d) 3D printer and components; (e,f) 3D printing of a unicompartimental capsule; (g) bicompartimental capsule; (h,i) parietal view of the 3D-printing process of Capsule@IRA-120-Cu(0) and Capsule@IRA-120-Pd(0); (j) view of the porous area (mesh) of Capsule@IRA-120-Pd(0). (k) View of Capsule@Amberlyst-15, in an isocyanide scavenging assay, in MeOH.

2.2.2. 3D Printing

Three-dimensional printing is not a new technology but is one of the most revolutionary. One can expect to witness upgrades of the existing design to arrive sooner than with any other technology. Therefore, 3D printing is an effective technology in prototyping processes. Fused deposition modeling (FDM) is one of the most widespread and easily accessible 3D-printing techniques [60]. Its realization begins with the reading of the file that contains the previously chosen design followed by the establishment of the printing conditions selected in advance. The printing process by FDM develops deposition of the selected material and superimposition layer by layer (Figure 2d). Polypropylene (PP) is a semicrystalline thermoplastic polymer with multiple applications thanks to its excellent combination of physicochemical properties, in addition to its relatively low price. Furthermore, PP has a high melting point (160 °C), a high resistance to flexing stress, low water absorption, good electrical and heat resistance, a lightweight, dimensional stability, high impact strength, and a nontoxicity property [61]. The fact that polypropylene contains only carbon and hydrogen atoms in its structure (Scheme 1d) implies that this material is only susceptible to being attacked by highly oxidizing agents and halogenated and aromatic solvents. This gives it high chemical resistance. Polypropylene will resist many organic solvents, acids, and alkalis. This material has a low density, which allows the manufacture of very light products. In addition, PP is considered a totally reusable and inert ecological material. Being a semicrystalline material, its crystalline phase provides its structural properties, as well as its rigidity, hardness, and tenacity, while its amorphous phase provides the viscoelastic properties such as its resistance to impacts. All these previously mentioned characteristics make PP a good resistant material to be used in solution chemistry. Nevertheless, a very important aspect is that 3D printing using PP is complicated, because this material has a low adhesion to the glass platforms of the printers. PP tends to stick to itself, but refuses to adhere to other materials, so printing it via FDM is challenging. For this reason, a membrane made of this same material with a minimum pore size was chosen, much less than 0.5 mm (Figure 2c,e), so that it allows the solvent to enter without letting the resin (average particle size of IRA-H: 0.6–0.8 mm, Amberlyst-15: <0.3 mm) pass into the medium reaction during its use in drug synthesis processes. Another noteworthy aspect of our procedure (see Section 3) is that both the selected technique (FDM) and the design of the capsule (bell-shaped or hemisphere) enable the complete fabrication of the device directly and easily in a single step (Figure 2e) while allowing the loading of the polymeric reagent inside (Figure 2f) in a quick process (approx. 20 min). Note that the sealing between the polypropylene membrane of the base (porous) and the capsule under construction occurs instantly, in the first minutes of the printing process. It is through the porous zone that the soluble reagents flow (Figure 2g).

2.2.3. Chemical and Mechanical Resistance Tests under SPOS Conditions

During the preliminary optimization stage, a series of capsule resistance tests were carried out against various solvent and temperature conditions. The great chemical and mechanical stability of PP [62] at high temperatures in a solution of methanol, water, and DMF was confirmed (Figure 2k). However, when solvents such as toluene or DCM were used, the capsule was damaged, so these devices cannot be used in chemical reactions that contain these solvents when working at high temperatures.

2.3. Preparation of Series 1 (Compounds 11–22): Ugi Reaction

Ugi compounds (Chart 1) were synthesized using similar conditions to those reported by Burke, Pineiro et al. [43]. These derivatives with unsubstituted NH at the isatin ring and halogen or alkyl substituents at position 5 reached cytotoxicity efficacies at the range of the most active reference compound, paclitaxel, against HBL-100 and HeLa cell lines. Specifically, this work aims to also report the activity of new diversely substituted isatins derived from the most potent structures reported previously [43] as cytotoxic agents (Scheme 2). Particularly, compound 12 showed potent antiproliferative activity in HBL-100 and HeLa

lines, thus being considered as the initial hit. Taking these results into account, which seem to suggest the importance of certain substituents at position 3 and 5 of the isatin ring, we selected a small library of promising target compounds to be tested in the murine 3T3-Balb fibroblast and human tumoral cervical HeLa cell lines containing these building blocks and, at the same time, verifying the effectiveness of the Capsule@Amberlyst-15-type resin (PS-TsOH) in the work-up processes for the elimination of excess isocyanide. The reactions proceeded satisfactorily in the presence of a Lewis acid-type catalyst (InCl_3) in methanol. In these transformations, we verified that the pKa of the acid component is key to the success of the reaction. Thus, reactions using trifluoroacetic acid work better and faster than those with chloroacetic acid. The reaction times and the yields are shown in Table 1. The expected Ugi-isatines 11–22 were also completely characterized by NMR experiments and compound 17 by single crystal X-ray analysis. Images of the ORTEP diagram corresponding to the crystalline structure are shown in Figure 3.

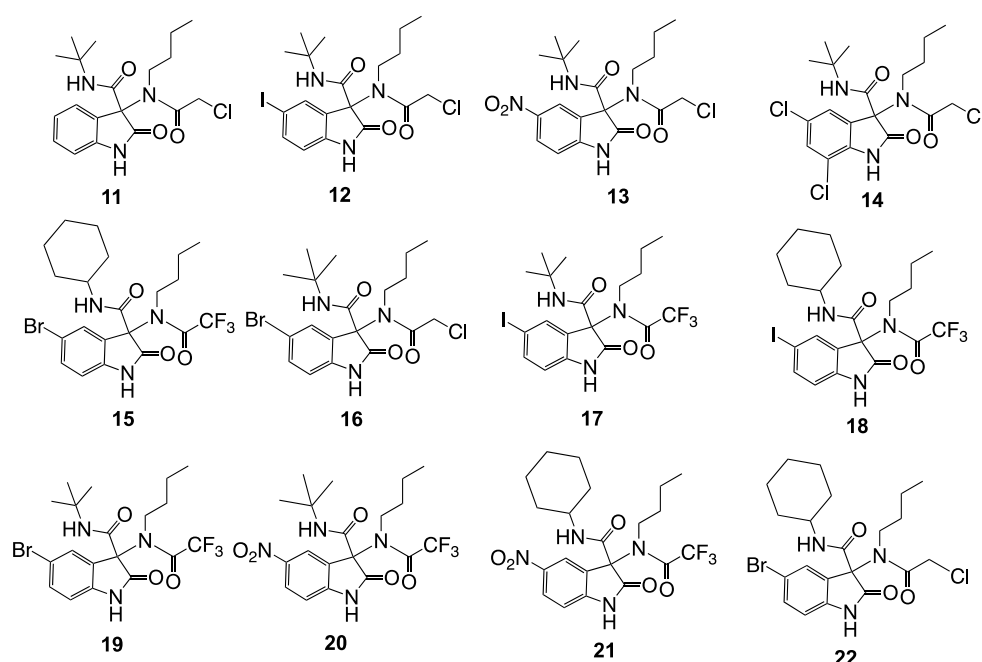


Chart 1. Chemical structures of the isatin compounds synthesized (series 1). Compounds 1: (X = H), 2 (X = I), 3 (X = Br), 4 (X = NO_2), 5 (X = Cl, X₇ = Cl).

Table 1. General conditions for the synthesis of the series 1 (compounds 11–22).

Compound	X ₅	Isocyanide	Acid	Time (h)	Yield (%) a,b,c
11	H	tert-butyl	ClCH_2COOH	48	65
12	I	tert-butyl	ClCH_2COOH	72	28
13	NO_2	tert-butyl	ClCH_2COOH	72	52
14	Cl (Cl = X ₇)	tert-butyl	ClCH_2COOH	72	30
15	Br	Cyclohexyl	CF_3COOH	48	58
16	Br	tert-butyl	ClCH_2COOH	72	21
17	I	tert-butyl	CF_3COOH	48	60
18	I	Cyclohexyl	CF_3COOH	48	55
19	Br	tert-butyl	CF_3COOH	48	58
20	NO_2	tert-butyl	CF_3COOH	48	55
21	NO_2	Cyclohexyl	CF_3COOH	48	57
22	Br	Cyclohexyl	ClCH_2COOH	72	42

^a Yield after purification. ^b All reactions used n-butylamine as the amino component, molecular sieves 3Å, rt.

^c All reactions were treated with Capsule@Amberlyst-15 for isocyanide scavenging.

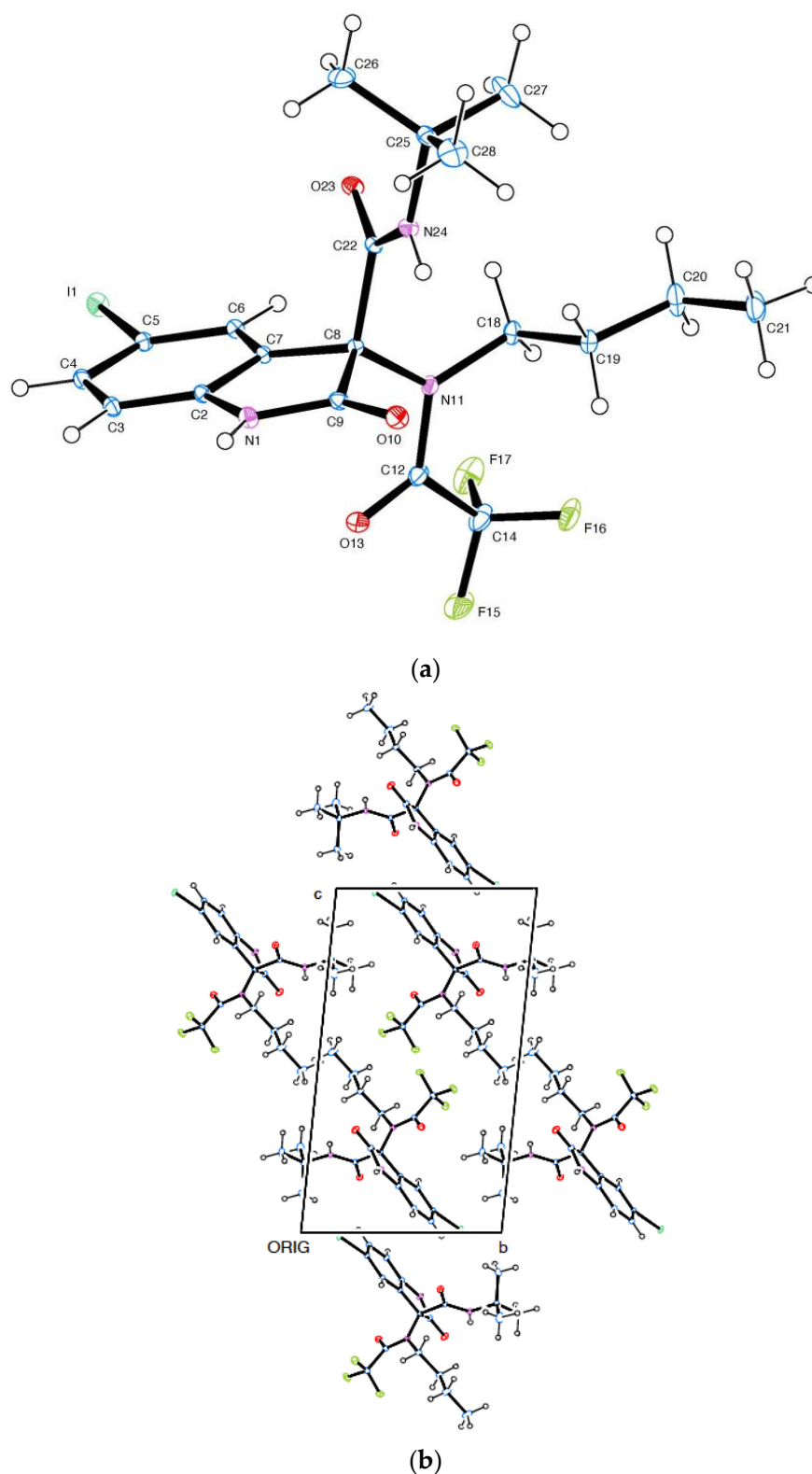


Figure 3. (a) ORTEP diagram of compound **17**, obtained by single crystal X-ray diffraction, showing the molecular conformation and numbering. (b) Crystal packing of **17**.

2.4. Capsule@Amberlyst-15 Behavior as Scavenger of Isocyanides, Post-Ugi Isocyanide Removal, Recycling of the Capsule after Scavenging

Scavenging process: The behavior of the Capsule@Amberlyst-15 capsule–resin pairing was evaluated during the work-up process for the removal of excess isocyanide. Once the

final product was formed, monitored by TLC, the scavenging process was carried out by directly immersing a semiporous polypropylene capsule containing the scavenger in the reaction medium, maintaining the mixture under magnetic stirring. Two equivalents of the supported *p*-TsOH led to complete elimination of the reactants under mild conditions. The process is relatively fast (30 min–1 h). After that interval, a complete absence of isocyanide odor is observed. After the process is complete, the capsule is removed from the flask with tweezers and washed with methanol.

Recycling process: The reactivation of the Capsule@Amberlyst-15 was carried out following a protocol described previously by our group [56]. After appropriate washing protocol (Figure 4d), the capsule containing the recovered sulfonate salt (formed after the scavenging process) was incubated in a 30% solution of trifluoroacetic acid in dichloromethane and submitted to orbital stirring for 1 h at room temperature (Figure 4). Once appropriately washed and dried under vacuum, the recovered immobilized capsule containing the *p*-toluenesulfonic acid supported reagent can be reused at least five times in new scavenging experiments for the same isocyanide without dramatic loss of effectiveness. Additionally, no apparent fracture or damage was detected in the capsule after treatment with dilute TFA.

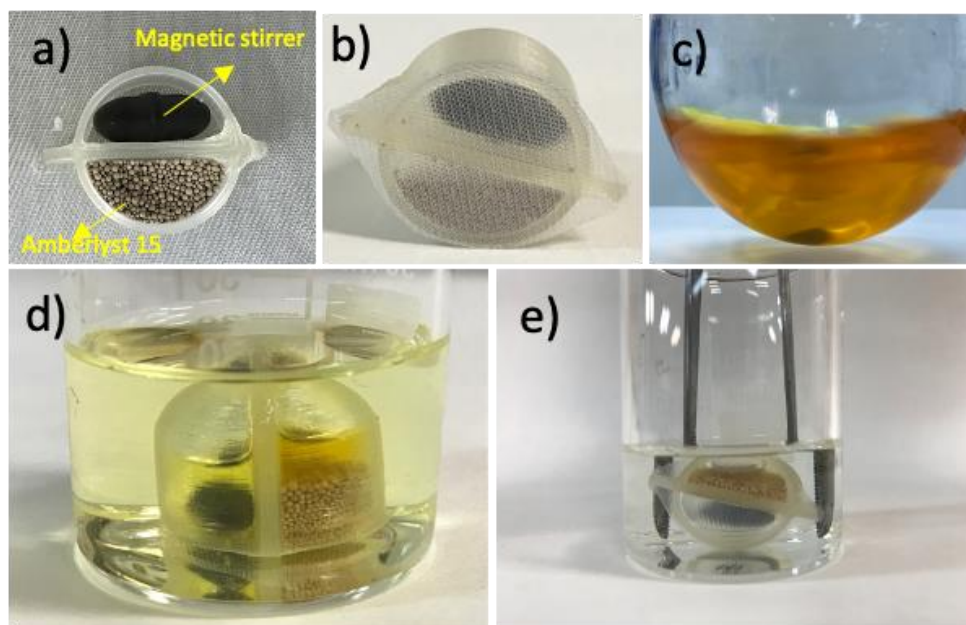


Figure 4. (a) Parietal view of the compartments during the 3D-printing process of capsule@Amberlyst-15 and the magnetic stirrer. (b) Bicompartimental 3D-printed Capsule@Amberlyst-15 finished, before scavenging. (c) Reaction mixture during treatment with Capsule@Amberlyst-15 polypropylene capsule. (d) Washing of the capsule after scavenging. (e) Capsule after TFA/DCM treatment, 1 h.

2.5. Preparation of Series 2 (Compounds 25–27) and 3 (Compounds 30–33)

The synthetic route to access new isatin-derived series 2 and 3 is shown in Scheme 3. The starting isatins were alkylated with propargyl bromide, benzyl bromide, or 4-iodobenzyl bromide to provide the key intermediates 23, 24, 28, and 29, respectively [47,63]. The CuAAC products, 25–27, were obtained by treating the starting alkynyl isatins with organic azides (benzyl azide or ethyl 2-azidoacetate) in the presence of a capsule containing the capsule@IRA-120-Cu(0), without the presence of other additives. The choice of the solvent was key: the starting isatins are not very soluble in EtOH or *t*BuOH at room temperature, although these solvents are frequently used in CuAAC [64] and compatible with capsule stability. Acetonitrile was optimal to obtain compounds 25–27 with good yields and in short reaction times, which demonstrates a correct flow of reagents within the capsule. In

this sense, a bicompartmental (internal magnetic stirrer) capsule shakes more vigorously than a unicompartmental one, accelerating the transformations inside the capsule.

The protocol for the synthesis of series 3 consisted of the preparation of four compounds derived from the dioxindoliny acrylate moiety. Three of them (**30**, **32**, **33**) were not previously described by Peng Yu et al. [47]. Thus, for the synthesis of compounds **30–33**, the Heck reaction for the alkenylation of halogenated positions assisted by the IRA-120-Pd(0) catalyst, loaded in a bicompartmental capsule (Figure 5) was used. The choice of the appropriate solvent (DMF/H₂O), base (sodium acetate), and temperature were crucial, since very high temperatures may damage both the capsule and the final isatin product itself, generating reaction byproducts.



Figure 5. (a) Heck reaction mixture using Capsule@IRA-120-Pd(0). (b) Capsule@IRA-120-Cu(0) during CuAAC. (c) Different shapes and sizes of 3D-printed capsule prototypes.

In the case of the synthesis of compound **30**, starting from N-protected isatin **2**, in addition to the Heck alkenylation in position 5, a 1,4-Aza-Michael addition occurs, promoted by deprotonation at N-1. For the synthesis of **31**, **32**, and **33**, precursors **28** and **29** were prepared, containing benzylic residues in position 1. The presence of a second iodine atom in the molecule, in para position of the benzylic ring, allows both obtaining the monoalkenylation product **32** and/or the double alkenylation product **33** (Table 2). The reactivity towards the iodo of C-5 to create compound **32** can be enhanced by conducting the reaction at moderate temperature (70 °C). On the contrary, a higher temperature (90 °C) and an excess of acrylate lead to a higher proportion of the bialkenylated compound **33**. Their structures were confirmed by ¹H NMR and ¹³C NMR as well as ESI-MS.

Table 2. Yields and methodologies for the target compounds 25–33.

Compound	Method	Catalyst	Time (h)	Yield (%) ^a
25	CuAAC ^b	IRA-120-Cu(0)	10	95
26	CuAAC ^b	IRA-120-Cu(0)	10	90
27	CuAAC ^b	IRA-120-Cu(0)	10	93
30	Aza-Michael/Heck ^{c,d}	IRA-120-Pd(0)	24	85
31	Heck ^c	IRA-120-Pd(0)	24	88
32	Heck ^c	IRA-120-Pd(0)	24	60 ^e
33	Heck ^d	IRA-120-Pd(0)	12	85

^a Yield after purification. ^b MeCN used as solvent, rt. ^c DMF/H₂O, 70 °C. ^d 90 °C. ^e 30% of compound **33** was formed.

2.6. Capsule Behavior and Reuse, Leaching Studies

These capsule devices have excellent resistance to the conditions of temperature (70–90 °C), reagents, and solvents required for the Heck reactions, as well as for CuAAC. In addition, the use of capsules facilitates the work-up process through extraction by tweezers. As can be seen in Figure 5, the shape and size of the 3D-printed prototypes are adapted to the dimensions of the desired flask. As can be seen in Figure 5c, it is possible to manufacture devices of different sizes and shapes. The bicompartmental capsules used in this work (25 × 17.7 × 19.6 mm) offer an approximate loading capacity of 900 mg of the three resins. Each capsule was reused in at least 5 new reactions without apparent loss of efficacy.

Interestingly, the polymer reagents contained in the capsules were inspected after 5 reaction cycles. The images taken under the microscope did not show significant changes in terms of the form of the supported reagents nor in the nanoparticle content. IRA-Pd(0) remained black while IRA-Cu(0) experienced a slight darkening of its copper color, probably as a consequence of a superficial oxidation process of copper. However, the recovery of the “zero” oxidation state for copper (clearly evidenced by the instantaneous color change) can easily be carried out by treatment with aqueous NaBH₄ (5 equiv.) for 1 h, at room temperature.

2.7. Biological Activity, Evaluation of Antiproliferative Activity

The cytotoxic activity of these new synthesized isatin derivatives was evaluated by means of the CCK8 antiproliferation assay *in vitro* in two different cell lines: cancerous cervical HeLa and murine 3T3 Balb fibroblast cells. The latter cell line is typically used to analyze the potential toxicity of (nano)materials thanks to their sensitivity. Figure 6 shows that isatins display a concentration-dependent cytotoxic profile. It can be observed that fibroblast cells were more sensitive to the presence of isatin derivatives than the cancerous cells in general HeLa ones, probably related to the enhanced replication rate of the tumoral cells. Analysis of the experimental data shown in Figure 6 allowed the determination of IC₅₀ values (see Tables 3 and 4). It is possible to discern two highly active molecules, compounds 26 and 33, with high specificity for tumoral cells and rather low half-inhibitory concentration values, IC₅₀ of 2.5 and 1.0 μM, respectively, and which is also much lower than those of Pt-based chemodrugs such as cisplatin (IC₅₀ = 15 μM) and carboplatin (IC₅₀ = 1.0 mM) currently used as first line treatment in clinics of primary cervical tumors. [65,66] Compounds 26 and 33 are, therefore, new promising hits for further development.

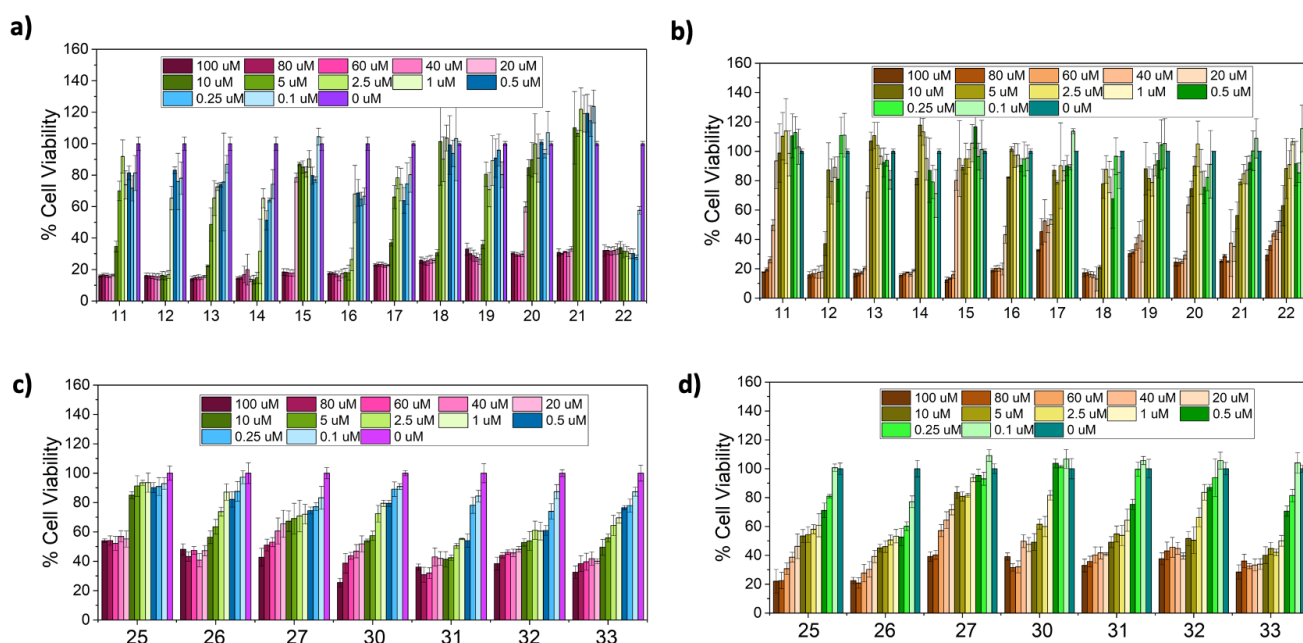


Figure 6. (a) Cell viability of Series 1 (compounds 11–22) in Balb and (b) HeLa cells. (c) Cell viability of Series 2 and 3 (compounds 25–33) in Balb and (d) HeLa cells.

Table 3. IC₅₀ (μM) values of the series 1 of isatin derivatives in murine fibroblast 3T3 and human cervical cancer cells.

Comp.	11	12	13	14	15	16	17	18	19	20	21	22
IC ₅₀ Balb (μM)	7.3 ± 0.7	1.3 ± 0.2	4.8 ± 0.9	1.5 ± 0.3	28.3 ± 1.7	1.5 ± 0.8	7.2 ± 0.5	8.5 ± 0.7	7.8 ± 0.4	25.0 ± 1.9	17.0 ± 0.7	0.12 ± 0.01
IC ₅₀ HeLa (μM)	40.1 ± 1.5	8.3 ± 0.8	26.9 ± 1.0	14.1 ± 0.3	47.7 ± 1.2	17.9 ± 1.3	33.0 ± 1.4	6.8 ± 0.5	16.8 ± 1.7	26.0 ± 1.9	12.4 ± 0.7	27.0 ± 0.8

Table 4. IC₅₀ (μM) values of the series 2 and 3 of isatin derivatives in murine fibroblast 3T3 and human cervical cancer cells.

Comp.	25	26	27	30	31	32	33
IC ₅₀ Balb (μM)	100 ± 3.1	21.5 ± 2.0	7.3 ± 0.7	42.1 ± 2.7	3.5 ± 0.8	32.1 ± 3.4	12.6 ± 0.9
IC ₅₀ HeLa (μM)	13.9 ± 4.5	2.5 ± 0.4	66.9 ± 8.9	9.3 ± 0.8	8.8 ± 1.1	10.8 ± 0.9	1.0 ± 0.05

Other drugs such as paclitaxel (IC₅₀ = 21 μM) and topotecan (IC₅₀ = 26 μM) [66,67] are used for the therapeutics of recurrent and metastatic cervical cancer. Moreover, there are another three compounds, **12**, **30**, and **31**, which despite not showing fully specific toxic activity for cancerous cells as occurred for many other potential chemotherapeutic compounds, they also have reduced IC₅₀ values of 8.3, 9.3, and 6.8 μM, respectively. Nevertheless, further studies are required to test the present synthesized isatin derivatives in other cancerous cells lines as toxicity profiles are known to depend on cell phenotype (see, for example, compounds **11**, **14**, and **22**), in addition to identifying the potential mechanism/s involved in cytotoxicity and subsequent cell death.

The data commented above, referring to the antiproliferative activity, allow us to draw some preliminary conclusions regarding the structure–activity relationships in these series. Thus, in series 1 (Ugi compounds), the maintenance of the chloroacetamide residue in position 3 seems to be important, as well as the presence of halogens (Br, I, Cl) in position 5 of isatin. With these characteristics, potent inhibition is achieved in at least one of the two cell lines studied, particularly for compound **22** (IC₅₀ = 0.12 μM in Balb Mur cell line) and **12** (IC₅₀: 1.3 μM in Balb and 8.3 μM in HeLa). Regarding the substituent from isocyanide (tert-butyl or cyclohexyl) from the Ugi reaction, both lyphophilic residues can provide good levels of antiproliferative activity, so this seems to be a less restrictive region.

Regarding series 2 and 3, we can conclude that the presence of a benzylic function on nitrogen is important for the activity in HeLa. In general, the aromatic moieties (benzene or 1,2,3-triazole) are conformationally flexible (see compounds **26** and **33**). The presence of an acrylate substituent in position 5 significantly improves potency (see compounds **31** and **33**). Substitution of the benzyl group by a short aliphatic chain containing an ester moiety does not improve activity (**31**). However, the presence of a 1,2,3-triazole ring in the place of benzene also seems to be very effective (**26**) when the halogen is kept at 5. New studies will be necessary to evaluate the best combination of substituents, both on the benzylic (or triazol) function as on position 5 of the isatin moiety, where both halogens (iodo) and the methyl acrylate-type residues are effective.

3. Materials and Methods

3.1. Chemistry: General Procedures for the Syntheses of the Catalytic Materials, Programs, Reagents, and Materials

Images of Pd nanoparticles dispersed in the polymer IRA-120 were acquired using a Gemini-500 field-emission scanning electron microscope (FESEM) operating at 20 kV using a back-scattering AsB detector with a size resolution of ±0.5 nm. Selected images were analyzed by counting more than 100 particles using ImageJ software. The surface morphology and microstructure of the samples were characterized using a scanning electron microscope

(SEM, JEOL 6400, JEOL Corporation, Japan) and a stereomicroscope (OlympusSZX12, Olympus, Japan). The surface elemental analysis of sintered samples was measured using an energy dispersive X-ray spectrometer (EDS, AZTEC/Xact, Oxford, UK).

Synthesis of IRA-120-Cu(0): Immobilization of copper (0) species on IRA-120H (1.8 mmol/g loading), support: Kimble vials in a PLS (6 × 4) organic synthesizer were used to load IRA-120H. First, IR-120 (1 g) was treated with 50 mL of NaOH 10% and stirred overnight at rt. The resulting light brown solution was filtered. The brown solid support IRA-120Na (0.5 g) was dried and then treated with a solution of CuSO₄ pentahydrate (25 mg, 0.1 mmol) in 10 mL of H₂O, and the suspension was vigorously stirred under orbital stirring at room temperature for 24 h. After this period, the blue color of the initial copper solution disappeared. The resulting green IRA-120-Cu(II) was filtered, washed with water, and dried under vacuum for 1 h at room temperature. The catalysts on the solid resin support were then filtered through a filter plate, washed, and transferred to a beaker with 50 mL of water. To this mixture, a fresh solution of 5 mL of NaBH₄ (1 mol/L) were added. The reduction was readily evidenced by the color change (copper color). IRA-120-Pd(0) catalytic system was prepared using the same procedure above but using Pd(AcO)₂ (20 mg) as metallic salt.

3.2. *Manufacture of Polypropylene Capsules by 3D Printing*

Tinkercad and CURA programs were used for the construction of the virtual 3D capsule. An Ultimaker 2+ extended 3D printer was used for the construction of the capsule, using the fused deposition modeling technique. A filament of polypropylene (2.85 mm diameter) was used as a 3D-printing material for the capsule. A piece of porous polypropylene membrane sheet was placed on the base and fixed to the base with a polypropylene film. The base conditions for the 3D printing of polypropylene (PP) capsules were the following. The platform was maintained at 40 °C. Nozzle diameter and temperature: 0.6 mm, 165 °C. The 3D-printed structure was sealed at the bottom by melting the borders of the polypropylene membrane during 3D printing. Once the printing of the capsule had begun (when the process reached 50% progress and the capsule walls had already formed, Figure S1 in the Supporting Information), the printing was paused briefly to fill the capsule with the IRA-120-Cu or Pd resin. Once the capsule was filled with the polymer reagent (and the magnetic stirrer in the case of bicompartimental capsules), 3D printing was resumed. To avoid melting or swelling of the thin polypropylene membrane located in the base, the temperature of the platform was maintained at 40 °C. The printing of the capsule was completed in 23 min (for dimensions: 25 × 17 × 19 mm).

3.3. *Chemistry, General Procedures for the Syntheses of the Series 1, 2, and 3*

Reagents and materials: Kimble vials in a PLS (6 × 4) organic synthesizer were used to perform the functionalization of IRA support with Pd and Cu species. Polystyrene-supported IRA-120H (1.8 mmol/g loading) and Amberlyst-15 (4.7 mmol/g loading) were purchased from Fluka. The rest of the reagents, methyl acrylate, isatins, InCl₃, were provided by Sigma-Aldrich. All reactions were monitored by TLC with 2.5 mm Merck silica gel GF 254 strips. The final purified compounds showed a single spot. Detection of compounds was performed by UV light and/or iodine vapor. Purification of isolated products was carried out by preparative TLC using silica gel plates. Characterization of the synthesized compounds was performed using spectroscopic and analytical data. The NMR spectra were recorded on Bruker AM 400 MHz (¹H) and 75 MHz (¹³C) and XM500 spectrometers. Chemical shifts are given as δ values against tetramethylsilane as the internal standard. J values are given in hertz. Proton and carbon nuclear magnetic resonance spectra were recorded in CDCl₃ or DMSO. Melting points were determined on a Gallenkamp apparatus and are uncorrected. Mass spectra were obtained on a Varian MAT-711 instrument. Mass spectra (ESI-MS) were obtained on an autospec micromass spectrometer. Crystallographic data of compound **17**: the data was measured with the Bruker D8 VENTURE PHOTON-III diffractometer using Mo radiation and at a temperature

of 100K. Computing details of data collection: Bruker APEX4 software; cell refinement: SAINT V8.40B (Bruker AXS LLC, 2019); data reduction: SAINT V8.40B (Bruker AXS LLC, 2019); program(s) used to solve structure: SHELXT 2018/2 (Sheldrick, 2015); program(s) used to refine structure: SHELXL2019/1 (Sheldrick, 2019); molecular graphics: ORTEP 2014.1 (Farrugia, 2012); software used to prepare material for publication: IUCr Journals pCIF (see Supplementary Material).

3.4. General Procedure for the Syntheses of Series 1 (Compounds 11–22)

The chemical library of Ugi-compounds was prepared by dissolving the corresponding isatin (**1–5**) (1 mmol), InCl_3 (10%), 100 mg of molecular sieves (3Å), *n*-butylamine (1.5 mmol), the acid component (1.5 mmol), and the isocyanide (1.5 mmol) in MeOH. After 48–72 h, CH_2Cl_2 (10 mL) and the bicompartmental Capsule@Amberlyst-15 (containing 900 mg of resin) were added. The mixture was stirred at rt for 1 h. Then, the capsule was extracted from the mixture, washed with MeOH and CH_2Cl_2 for reuse in further reactions after reactivation. After solvent removal under reduced pressure, the crude product was crystallized from ethanol or purified by preparative TLC ($\text{CH}_2\text{Cl}_2/\text{MeOH}$). Reactivation of bicompartmental Capsule@IRA-Amberlyst-15: The reagent-containing capsule was treated with 30 mL of a TFA/ CH_2Cl_2 (30%) solution for 3 h while stirring and at room temperature.

Compound N-(tert-butyl)-3-(N-butyl-2-chloroacetamido)-1-methyl-2-oxoindoline-3-carboxamide (**11**) was obtained as a white solid (316.8 mg, 65% yield). m.p. = 144.1–145.0 °C. ^1H NMR (CDCl_3 , 400 MHz): δ 7.48 (d, J = 7.0 Hz, 1H), 7.32 (td, J = 7.7, 1.1, 1H), 7.18 (br, 1H), 7.10 (td, J = 7.6, 0.7 Hz, 1H), 6.84 (d, J = 7.8 Hz, 1H), 4.09 (dd, J = 13.0 Hz, 2H), 3.69–3.3.61 (m, 1H), 3.59–3.50 (m, 1H), 3.26 (s, 3H), 1.94–1.84 (m, 1H), 1.74–1.63 (m, 1H), 1.36–1.30 (m, 11H), 0.95 (t, J = 7.4 Hz, 3H). MS (ESI) [M-H]: 378 [43].

Compound N-(tert-butyl)-3-(N-butyl-2-chloroacetamido)-5-iodo-2-oxoindoline-3-carboxamide (**12**) was obtained as a yellow solid (102.9 mg, 28% yield). m.p. = 108.5–109.7 °C. ^1H NMR (CDCl_3 , 400 MHz): δ 8.11 (br s, 1H), 7.68 (d, J = 1.6 Hz, 1H), 7.54 (dd, J = 8.2, 1.7 Hz, 1H), 7.17 (br s, 1H), 6.60 (d, J = 8.2 Hz, 1H), 4.17 (d, J = 13.2 Hz, 1H), 4.10 (d, J = 13.1 Hz, 1H), 3.70–3.62 (m, 1H), 3.58–3.50 (m, 1H), 1.97–1.86 (m, 1H), 1.78–1.67 (m, 1H), 1.37–1.30 (m, 11H), 0.99 (t, J = 7.3 Hz, 3H). MS (ESI) [M-H]: 504 [43].

Compound N-(tert-butyl)-3-(N-butyl-2-chloroacetamido)-5-nitro-2-oxoindoline-3-carboxamide (**13**) was obtained as a white solid (230.7 mg, 52% yield). m.p. = 179.5–179.8 °C. ^1H NMR (CDCl_3 , 400 MHz): δ 8.67 (br s, 1H), 8.29 (d, J = 2.2 Hz, 1H), 8.21 (dd, J = 8.6, 2.3 Hz, 1H), 7.16 (br s, 1H), 6.90 (d, J = 8.6 Hz, 1H), 4.24 (d, J = 13.3 Hz, 1H), 4.12 (d, J = 13.3 Hz, 1H), 3.76–3.68 (m, 1H), 3.66–3.58 (m, 1H), 2.10–1.99 (m, 1H), 1.88–1.76 (m, 1H), 1.42 (q, J = 7.4 Hz, 2H), 1.35 (s, 9H), 1.04 (t, J = 7.3 Hz, 3H). MS (ESI) [M-H]: 423 [43].

Compound N-(tert-butyl)-3-(N-butyl-2-chloroacetamido)-5,7-dichloro-2-oxoindoline-3-carboxamide (**14**) was obtained as a white-yellow solid (30% yield). m.p. = 125–126 °C. ^1H NMR (CDCl_3 , 400 MHz): δ 8.94 (br, 1H, NH), 7.43 (s, 1H), 7.38 (s, 1H), 4.28 (dd, J = 9.5, 1.2 Hz, 2H), 3.80–3.64 (m, 2H), 2.05 (m, 1H), 188 (m, 1H), 1.59–1.40 (m, 12H), 1.15–1.05 (m, 4H). ^{13}C NMR (CDCl_3 , 75.4 MHz): δ 174.6, 167.1, 159.9, 137.5, 128.9, 128.7, 115.7, 109.2, 73.1, 52.5, 47.1, 41.4, 33.8, 31.2, 28.1, 19.9, 13.5. MS (ESI) [M-H]: 446.

Compound 5-bromo-3-(N-butyl-2,2,2-trifluoroacetamido)-*N*-cyclohexyl-2-oxoindoline-3-carboxamide (**15**) was obtained as a white-yellow solid (58% yield). m.p. = 209–210 °C. ^1H NMR (CDCl_3 , 400 MHz): δ 8.91 (br, 1H), 7.59 (s, 1H), 7.37 (dd, J = 8.3, 2.1 Hz, 1H), 6.96 (d, J = 7.8 Hz, 1H), 6.69 (d, J = 8.2 Hz, 1H), 3.86–3.55 (m, 3H), 1.94–1.14 (m, 14H), 0.92 (t, J = 7.4 Hz, 3H). ^{13}C NMR (CDCl_3 , 75.4 MHz): δ 173.8, 160.1, 140.1, 132.9, 129.3, 127.2, 117.3, 116.1, 114.5, 112.0, 72.1, 49.7, 46.9, 33.3, 32.1, 32.1, 25.3, 24.5, 24.4, 19.8, 13.3. MS (ESI) [M-H]: 503.

Compound 5-Bromo-N-(tert-butyl)-3-(N-butyl-2-chloroacetamido)-2-oxoindoline-3-carboxamide (**16**) was obtained as a pale-yellow solid (85.6 mg, 21% yield). m.p. = 180–182 °C. ^1H NMR (CDCl_3 , 400 MHz): δ 8.14 (br s, 1H), 7.52 (d, J = 1.8 Hz, 1H), 7.35 (dd, J = 8.3, 2.0 Hz, 1H), 7.17 (br s, 1H), 6.69 (d, J = 8.3 Hz, 1H), 4.18 (d, J = 13.1 Hz, 1H), 4.10 (d, J = 13.1 Hz,

1H), 3.70–3.62 (m, 1H), 3.59–3.50 (m, 1H), 1.99–1.88 (m, 1H), 1.79–1.68 (m, 1H), 1.39–1.34 (m, 11H), 0.99 (t, $J = 7.3$ Hz, 3H). MS (ESI) [M-H]: 457 [43].

Compound *N*-(*tert*-butyl)-3-(*N*-butyl-2,2,2-trifluoroacetamido)-5-iodo-2-oxoindoline-3-carboxamide (**17**) was obtained as a white solid (60% yield). m.p.= 204–205 °C. ¹H NMR (CDCl₃, 400 MHz): δ 8.50 (br s, 1H), 7.72 (s, 1H), 7.58 (dd, $J = 8.2, 1.7$ Hz, 1H), 7.01 (s, 1H), 6.60 (d, $J = 8.2$ Hz, 1H), 3.81 (m, 1H), 3.61 (m, 1H), 1.94 (m, 1H), 1.68 (m, 1H), 1.32 (m, 11H), 0.95 (t, $J = 7.4$ Hz, 3H). ¹³C NMR (CDCl₃, 75.4 MHz): δ 174.0, 159.5, 157.7, 140.7, 138.7, 135.1, 127.5, 117.3, 112.4, 86.1, 72.5, 52.6, 46.9, 33.5, 28.1, 19.9, 13.4. MS (ESI) [M-H]: 526.

Compound 3-(*N*-butyl-2,2,2-trifluoroacetamido)-*N*-cyclohexyl-5-iodo-2-oxoindoline-3-carboxamide (**18**) was obtained as a white-yellow solid (55% yield). m.p.= 218–220 °C. ¹H NMR (CDCl₃, 400 MHz): δ 8.70 (s, 1H), 7.75 (s, 1H), 7.57 (dd, $J = 8.2, 1.7$ Hz, 1H), 6.96 (d, $J = 7.8$ Hz, 1H), 6.58 (d, $J = 8.2$ Hz, 1H), 3.86–3.55 (m, 3H), 1.95–1.14 (m, 14H), 0.92 (t, $J = 7.4$ Hz, 3H). ¹³C NMR (CDCl₃, 75.4 MHz): δ 173.6, 160.1, 157.4, 140.7, 138.8, 134.9, 127.5, 117.5, 117.3, 112.4, 86.1, 71.9, 49.7, 46.8, 33.3, 32.1, 32.1, 25.3, 24.5, 24.4, 19.8, 13.4. MS (ESI) [M-H]: 550.

Compound 5-bromo-*N*-(*tert*-butyl)-3-(*N*-butyl-2,2,2-trifluoroacetamido)-2-oxoindoline-3-carboxamide (**19**) was obtained as a white solid (58% yield). m.p.= 198–200 °C. ¹H NMR (CDCl₃, 400 MHz): δ 8.37 (br s, 1H), 7.57 (s, 1H), 7.39 (dd, $J = 8.3, 2.0$ Hz, 1H), 7.01 (s, 1H), 6.70 (d, $J = 8.2$ Hz, 1H), 3.82 (m, 1H), 3.62 (m, 1H), 1.96 (m, 1H), 1.69 (m, 1H), 1.32 (m, 11H), 0.95 (t, $J = 7.4$ Hz, 3H). ¹³C NMR (CDCl₃, 75.4 MHz): δ 174.1, 159.5, (151.0), 140.1, 132.8, 129.5, 127.2, 116.1, 112.0, 86.1, 72.7, 52.6, 46.9, 33.5, 28.1, 19.8, 13.4. MS (ESI) [M-H]: 477.

Compound *N*-(*tert*-butyl)-3-(*N*-butyl-2,2,2-trifluoroacetamido)-5-nitro-2-oxoindoline-3-carboxamide (**20**) was obtained as a white solid (55% yield). m.p.= 178–180 °C. ¹H NMR (CDCl₃, 400 MHz): δ 8.89 (br, 1H), 8.33 (d, $J = 2.3$ Hz, 1H), 8.23 (dd, $J = 8.7, 2.3$ Hz, 1H), 7.06 (s, 1H), 6.94 (d, $J = 8.6$ Hz, 1H), 3.87 (m, 1H), 3.67 (m, 1H), 2.09 (m, 1H), 1.79 (m, 1H), 1.35 (m, 11H), 1.00 (t, $J = 7.4$ Hz, 3H). ¹³C NMR (CDCl₃, 75.4 MHz): δ 174.9, 158.5, 146.5, 144.2, 126.6, 126.1, 122.5, 117.2, 114.34, 110.3, 72.3, 523.0, 47.1, 33.7, 28.1, 19.9, 13.4. MS (ESI) [M-H]: 443.

Compound 3-(*N*-butyl-2,2,2-trifluoroacetamido)-*N*-cyclohexyl-5-nitro-2-oxoindoline-3-carboxamide (**21**) was obtained as a pale-yellow solid (57% yield). m.p.= 200–202 °C. ¹H NMR (CDCl₃, 400 MHz): δ 8.98–8.78 (br, 1H), 8.36 (s, 1H), 8.22 (dd, $J = 8.7, 2.3$ Hz, 1H), 7.05 (d, $J = 7.8$ Hz, 1H), 6.90 (d, $J = 8.6$ Hz, 1H), 3.95–3.61 (m, 3H), 1.98–1.18 (m, 14H), 0.98 (t, $J = 7.4$ Hz, 3H). ¹³C NMR (CDCl₃, 75.4 MHz): δ 174.6, 158.9, 146.6, 144.1, 144.1, 126.6, 126.1, 122.3, 117.2, 114.3, 110.3, 71.7, 50.0, 47.1, 33.5, 32.1, 25.2, 24.5, 24.4, 19.9, 13.4. MS (ESI) [M-H]: 469.

Compound 5-bromo-3-(*N*-butyl-2-chloroacetamido)-*N*-cyclohexyl-2-oxoindoline-3-carboxamide (**22**) was obtained as a beige solid (42% yield). m.p.= 190.2–190.4 °C. ¹H NMR (CDCl₃, 300 MHz): δ 8.65 (s, 1H), 7.54 (s, 1H), 7.33 (dd, $J = 8.3, 2.0$ Hz, 1H), 7.16 (d, $J = 7.8$ Hz, 1H), 6.66 (d, $J = 8.3$ Hz, 1H), 4.15 (q, $J = 13.2$ Hz, 2H), 3.73–3.46 (m, 3H), 1.95–1.15 (14H), 0.97 (t, $J = 7.3$ Hz, 3H). ¹³C NMR (CDCl₃, 75.4 MHz): δ 174.8, 167.1, 160.9, 140.2, 132.3, 129.1, 128.2, 115.7, 111.9, 71.8, 49.5, 47.2, 41.62, 33.6, 32.2, 25.3, 24.5, 24.5, 20.1, 13.5. MS (ESI) [M-H]: 483.

3.5. General Procedures for the Syntheses of the Intermediates for Series 2 and 3

To a solution of isatins **1** and **2** (1 mmol) was added anhydrous K₂CO₃ (1.5 mmol, 207 mg) in anhydrous acetonitrile (10 mL) in a microwave vessel. Propargyl bromide (1.5 mmol, 0.167 mL of solution 80 wt% in toluene) was then added dropwise into the suspension mixture. The reaction mixture was heated under reflux while stirring at 50 °C for 12 h. When the reaction was accomplished (monitored by TLC.), the solvent was evaporated completely under reduced pressure at 50 °C. After the reaction was completed, the mixture was cooled to room temperature, and water was added to the mixture to dissolve inorganic salts (K₂CO₃ and KBr) and extracted with ethyl acetate and dried with

anhydrous sodium sulfate. The solvent was removed under reduced pressure. The residue was crystallized from ethanol to afford the title substituted N-propargyl isatins **23** or **24** [63].

Compound **23** was obtained as an orange solid (80% yield). m.p.= 156–158 °C. ¹H NMR (CDCl₃, 400 MHz): δ 7.65 (m, 2H), 7.14 (m, 2H), 4.53 (s, 2H), 2.31 (s, 1H). ¹³C NMR (CDCl₃, 75.4 MHz MHz): δ 182.5, 157.1, 149.6, 138.4, 125.4, 124.2, 117.7, 111.1, 75.6, 73.3, 29.4. MS (ESI) [M + H]: 186.0.

Compound **24** was obtained as an orange solid (85% yield). m.p.= 110–112 °C. ¹H NMR (CDCl₃, 400 MHz): δ 7.92 (m, 2H), 6.95 (m, 1H), 4.52 (s, 2H), 2.32 (s, 1H). ¹³C NMR (CDCl₃, 75.4 MHz MHz): δ 181.1, 156.1, 148.8, 146.4, 133.9, 119.2, 113.2, 86.6, 75.2, 73.7, 29.5. MS (ESI) [M + H]: 311.90.

To a solution of isatin **2** (1 mmol) was added anhydrous K₂CO₃ (1.5 mmol, 207 mg) in anhydrous acetonitrile (10 mL) in a microwave vessel. Benzyl bromide or 4-iodo-benzyl bromide (1.5 mmol) was then added dropwise into the suspension mixture. The reaction mixture was heated under reflux while stirring at 50 °C for 12 h. When the reaction was accomplished (monitored by TLC.), the solvent was evaporated completely under reduced pressure at 50 °C. After the reaction was completed, the mixture was cooled to room temperature, and water was added to the mixture to dissolve inorganic salts (K₂CO₃ and KBr) and extracted with ethyl acetate and dried with anhydrous sodium sulfate. The solvent was removed under reduced pressure. The residue was crystallized from ethanol to afford the title substituted N-benzyl isatins **28** or **29**.

Compound **28** was obtained as an orange solid (90% yield). m.p.= 200–201 °C. ¹H NMR (CDCl₃, 400 MHz): δ 7.86 (m, 2H), 7.53 (s, 1H), 7.38–7.18 (m, 6H), 5.48 (s, 2H), 4.97 (s, 2H). ¹³C NMR (CDCl₃, 75.4 MHz MHz): δ 181.7, 157.2, 149.6, 146.4, 138.3, 134.0, 133.7, 129.2, 119.2, 112.9, 93.9, 86.4, 43.6. MS (ESI) [M + H]: 321.33.

Compound 1-benzyl-5-iodoindoline-2,3-dione (**29**) was obtained as an orange solid (90% yield). m.p.= 198–200 °C. ¹H NMR (CDCl₃, 400 MHz): δ 7.89 (d, *J* = 1.8 Hz, 1H), 7.77 (d, *J* = 8.3 Hz, 1H), 7.40–7.24 (m, 5H), 6.57 (d, *J* = 8.3 Hz, 1H), 4.92 (s, 2H). ¹³C NMR (CDCl₃, 75.4 MHz MHz): δ 181.9, 157.2, 159.0, 146.3, 134.0, 133.8, 129.1, 128.3, 127.4, 119.2, 113.1, 86.2, 44.1. MS (ESI) [M + H]: 363.

3.6. General Procedures for the Syntheses of the Serie 2 (CuAAC Reaction)

In a round-bottomed flask, alkynyl isatin **23** (400 mg, 1 mmol) was dissolved in acetonitrile (10 mL). Then, benzyl azide (1.1 mmol) and Capsule@IRA-120-Cu(0) (containing 100 mg of resin, containing 21% Cu) were added. The reaction was left stirred at room temperature for 10 h. The reaction was monitored by TLC. Once the complete transformation of the starting product was verified, the capsule was removed from the reaction medium with tweezers and washed with acetonitrile for reuse. The organic solution used for washing the capsule was combined with the rest of the reaction mixture and evaporated to dryness in a rotary evaporator. The resulting solid was recrystallized from iPrOH to create **25**.

Compound **25** was obtained as an orange solid (95% yield). m.p.= 175–177 °C. ¹H NMR (CDCl₃, 400 MHz): δ 7.51–6.99 (m, 10H), 5.41 (s, 2H), 4.91 (s, 2H). ¹³C NMR (CDCl₃, 75.4 MHz MHz): δ 183.1, 158.1, 150.3, 142.0, 138.6, 134.0, 129.2, 129.0, 128.3, 125.3, 124.0, 123.2, 117.6, 111.6, 54.7, 35.4. MS (ESI) [M + H]: 319.1.

Compound **26** was obtained as an orange solid (90% yield). m.p.= 183–185 °C. ¹H NMR (CDCl₃, 400 MHz): δ 7.86 (m, 2H), 7.53 (s, 1H), 7.38–7.18 (m, 6H), 5.48 (s, 2H), 4.97 (s, 2H). ¹³C NMR (CDCl₃, 75.4 MHz MHz): δ 181.7, 156.9, 149.5, 146.7, 142.0, 133.8, 133.7, 129.3, 129.1, 128.3, 123.0, 119.0, 113.8, 86.4, 54.6, 35.3. MS (ESI) [M + H]: 311.08.

Compound **27** was obtained as a red solid (93% yield). m.p.= 158–159 °C. ¹H NMR (CDCl₃, 400 MHz): δ 7.86–7.80 (m, 3H), 7.12 (dd, *J* = 8.3, 0.6 Hz, 1H), 5.13 (s, 2H), 5.00 (s, 2H), 4.23 (q, *J* = 7.1 Hz, 2H), 1.26 (t, *J* = 7.1 Hz, 3H). ¹³C NMR (CDCl₃, 75.4 MHz MHz): δ 181.7, 165.9, 156.9, 149.5, 146.6, 133.7, 133.6, 124.5, 119.0, 113.7, 86.4, 62.5, 50.9, 35.4, 14.0. MS (ESI) [M + H]: 441.

3.7. Syntheses of the Series 3 (Heck Reaction)

In a round bottom flask, 400 mg (1 mmol) of 5-iodoisatin **29** was dissolved in DMF (10 mL). To this solution was added another aqueous solution of sodium acetate (3 mmol in 1.5 mL of water), methyl acrylate (1.5 mmol), and Capsule@IRA-120-Pd(0) (100 mg of resin, containing 22% of Pd). The reaction was kept stirring at 90 °C for 12 h. The reaction was monitored by TLC until complete consumption of the starting product. Once the reaction was finished, the capsule was extracted from the reaction medium and washed (MeOH, water, AcOEt) for reuse. The reaction mixture was diluted with AcOEt (30 mL) and washed with water (10 mL), and the solvent was evaporated in a rotavapor at 50 °C, and the residue was purified on preparative TLC to create compound **31**.

Compound 1-benzyl-5-iodoindoline-2,3-dione **31** was obtained as a red solid (88% yield). m.p.= 164–165 °C. ¹H NMR (CDCl₃, 400 MHz): δ 7.70 (d, *J* = 1.8 Hz, 1H), 7.57–7.46 (m, 2H), 7.30–7.19 (m, 5H), 6.74 (d, *J* = 8.2 Hz, 1H), 6.27 (d, *J* = 16.0 Hz, 1H), 4.88 (s, 2H), 3.72 (s, 3H). ¹³C NMR (CDCl₃, 75.4 MHz): δ 182.6, 166.9, 158.1, 151.5, 142.4, 138.0, 134.1, 130.5, 129.1, 128.3, 127.4, 124.1, 118.2, 119.0, 111.4, 51.8, 44.2. MS (ESI) [M + H]: 322.3.

In a round bottom flask, 400 mg (1 mmol) of 5-iodoisatin **29** was dissolved in DMF (10 mL). To this solution was added another aqueous solution of sodium acetate (3 mmol in 1.5 mL of water), methyl acrylate (1.2 mmol), and Capsule@IRA-120-Pd(0) (100 mg of resin, containing 22% of Pd). The reaction was kept stirring at 70 °C for 24 h. The reaction was monitored by TLC until complete consumption of the starting product. Once the reaction was finished, the capsule was extracted from the reaction medium and washed (MeOH, water, AcOEt) for reuse. The reaction mixture was diluted with AcOEt (30 mL) and washed with water (10 mL), and the solvent was evaporated in a rotavapor at 50 °C, and the residue was purified on preparative TLC to create compound **32**.

Compound methyl (E)-3-(1-(4-iodobenzyl)-2,3-dioxindolin-5-yl)acrylate **32** was obtained as a red solid (60% yield). m.p.= 228–230 °C. ¹H NMR (CDCl₃, 400 MHz): 7.79 (d, *J* = 1.7 Hz, 1H), 7.69 (d, *J* = 8.3 Hz, 1H), 7.69–7.60 (m, 2H), 7.58 (d, *J* = 16.0 Hz, 1H), 7.11 (m, 1H), 7.08 (d, *J* = 8.4 Hz, 1H), 6.78 (d, *J* = 8.2 Hz, 1H), 6.36 (d, *J* = 16.0 Hz, 1H), 4.89 (s, 2H), 3.80 (s, 3H). ¹³C NMR (CDCl₃, 75.4 MHz): δ 182.3, 166.9, 158.1, 151.7, 142.3, 138.3, 138.0, 133.8, 130.8, 129.3, 124.2, 118.4, 118.1, 111.2, 93.9, 51.9, 43.8. MS (ESI) [M + H]: 448.0.

In a round bottom flask, 400 mg (1 mmol) of iodoisatin **29** was dissolved in DMF (10 mL). To this solution was added another aqueous solution of sodium acetate (6 mmol in 2 mL of water), methyl acrylate (3 mmol), and Capsule@IRA-120-Pd(0) (100 mg of resin, containing 22% of Pd). The reaction was kept stirring at 90 °C for 12 h. The reaction was monitored by TLC until complete consumption of the starting product. Once the reaction was finished, the capsule was extracted from the reaction medium and washed (MeOH, water, AcOEt) for reuse. The reaction mixture was diluted with AcOEt (30 mL) and washed with water (10 mL), and the solvent was evaporated in a rotavapor at 50 °C and, the residue was purified on preparative TLC to create compound **33**.

Compound methyl (E)-3-(4-((E)-3-methoxy-3-oxoprop-1-en-1-yl)-2,3-dioxindolin-1-yl)methyl)phenyl)acrylate **33** was obtained as a red solid (85% yield). m.p. = 188–190 °C. ¹H NMR (CDCl₃, 400 MHz): δ 7.80–7.50 (m, 6H), 7.40 (br, 1H), 7.35 (d, *J* = 8.0 Hz, 1H), 6.79 (d, *J* = 8.2 Hz, 1H), 6.44–6.33 (m, 2H), 4.96 (s, 2H), 3.80 (s, 6H). ¹³C NMR (CDCl₃, 75.4 MHz): δ 182.4, 167.2, 166.9, 158.1, 151.2, 143.7, 142.3, 138.0, 136.2, 134.6, 130.8, 128.8, 127.9, 124.3, 118.6, 118.4, 118.1, 111.2, 51.9, 51.8, 43.9. MS (ESI) [M + H]: 406.0.

3.8. Procedure for the Syntheses of Compound **30**

In a round bottom flask, 400 mg (1 mmol) of 5-iodoisatin **2** was dissolved in DMF (10 mL). To this solution was added another aqueous solution of sodium acetate (3 mmol in 1.5 mL of water), methyl acrylate (3 mmol), and Capsule@IRA-120-Pd(0) (100 mg of resin, containing 22% of Pd). The reaction was kept stirring at 90 °C for 24 h. The reaction was monitored by TLC until complete consumption of the starting product. Once the reaction was finished, the capsule was extracted from the reaction medium and washed (MeOH, water, AcOEt) for reuse. The reaction mixture was diluted with AcOEt (30 mL) and washed

with water (10 mL), and the solvent was evaporated in a rotavapor at 50 °C, and the residue was purified on preparative TLC to create compound **30**.

Compound methyl (E)-3-(1-(3-methoxy-3-oxopropyl)-2,3-dioxindolin-5-yl)acrylate **31** was obtained as a red solid (85% yield). m.p.= 131–132 °C. ¹H NMR (CDCl₃, 400 MHz): δ 7.74–7.71 (m, 2H), 7.58 (d, *J* = 16.0 Hz, 1H), 7.12–7.06 (m, 1H), 6.36 (d, *J* = 16.0 Hz, 1H), 4.03 (t, *J* = 6.8 Hz, 2H), 3.78 (s, 3H), 3.65 (s, 3H), 2.76 (t, *J* = 6.8 Hz, 2H). ¹³C NMR (CDCl₃, 75.4 MHz): δ 182.4, 171.2, 166.9, 158.2, 151.3, 142.3, 138.0, 130.4, 124.1, 118.1, 117.9, 110.9, 52.1, 51.8, 36.4, 31.9. MS (ESI) [*M* + *H*]: 317.29.

3.9. Cell Cultures

Cervical HeLa cancer cells and 3T3 mouse fibroblasts from Cell Biolabs (San Diego, CA, USA) were grown in standard culture conditions (5% CO₂ at 37 °C) in DMEM supplemented with 10% (*v/v*) FBS, 2 mM L-glutamine, 1% (*v/v*) penicillin/streptomycin, 1 mM sodium pyruvate, and 0.1 mM MEM nonessential amino acids (NEAA).

3.10. In Vitro Cell Cytotoxicity

Cytotoxicity of the synthesized isatin-based compounds was tested in vitro by means of the CCK-8 cytotoxicity assay. Cancerous cervical HeLa and 3T3 Balb fibroblasts cells were seeded into 96-well plates (1.0 × 10⁴ cells/well) and grown for 24 h at an optical confluence of 80–90% under standard culture conditions in 100 μL growth medium. Bare cells were used as the negative control. After 24 h of incubation at 37 °C, 100 μL of NPs at 2.5 × 10¹⁰ NP/mL in the corresponding cell culture medium were injected into the wells and incubated for 24 h and 48 h. After incubation, the culture medium was discarded, cells were washed with 10 mM PBS (pH 7.4) several times, and fresh culture medium (100 μL) containing 10 μL of CCK-8 reagent added to each well. After 2 h, the absorption at 450 nm of cell samples was measured with an UV-vis microplate absorbance reader (Bio-Rad model 689, USA). Cell viability (SR, survival rate) was calculated as follows:

$$SR = \frac{Abs_{sample}}{Abs_{blank}} \times 100$$

where *Abs_{sample}* is the absorbance at 450 nm for cell samples, and *Abs_{blank}* is the absorbance corresponding to the sample controls without the particles.

For the determination of the half-maximal inhibitory concentration (IC₅₀), a dose-response curve between the isatin derivatives' concentrations and percent cell viability was plotted and fitted by means of a nonlinear least-squares fitting method (Microcal Origin 2021) to a four-parameter logistic equation:

$$Y = min + \left(\frac{(max - min)}{1 + 10^{((logIC_{50} - X) \times p)}} \right)$$

where the original, %control or %survival data are represented by *Y* along their minimal (*min*) and maximal (*max*) values; the isatin derivative concentration is represented by *X*; IC₅₀ is the concentration at 50% maximal value; and *p* is the slope factor.

4. Conclusions

The compartmentalization of solid reagents and catalysts is an interesting strategy that enables not only their easy dispensability and reuse in work-up processes, but also their simultaneous use in chemical reactions, even those in which they are incompatible. Particularly interesting for the pharmaceutical industry is the application of compartmentalized reagents in complex reactions that generate new bioactive heterocyclic structures.

In this work, we have demonstrated for the first time the applicability of the 3D-printing technology in the construction of custom capsule-shaped devices, made of polypropylene, and their integration and application in drug synthesis. These prototypes were tested in SPOS-type reactions as effective systems to compartmentalize supported polymeric reagents,

in general, and polymeric catalysts containing metal species, specifically. These devices demonstrated efficacy as containers for the Amberlyst-15 acid reagent as a scavenger of isocyanides in Ugi work-up processes and/or for the IRA-120-Cu(0) and IRA-120-Pd(0) catalysts, in CuAAC- or Heck-type reactions, respectively. These reactions gave rise to the synthesis of different series of diversely substituted isatins, which showed potent activity as antiproliferative agents in HeLa and murine 3T3 Balb fibroblast cell lines.

Supplementary Materials: The following supporting information can be downloaded at: <https://www.mdpi.com/article/10.3390/ph16020310/s1>, Figure S1; RMN and mass spectra of the related compounds.

Author Contributions: Conceptualization, A.C.; methodology, A.C., C.C., O.B., M.L., S.B. and C.M.; software, A.C.; validation, J.M.B.; investigation, C.M., O.B. and M.L.; resources, P.T.; data curation, M.A., C.C., O.B., M.L. and S.B.; writing—original draft preparation, A.C.; writing—review and editing, A.C. and P.T.; visualization, C.M.; supervision, M.A., J.M.B. and C.F.M.; project administration, A.C.; funding acquisition, P.T. and A.C. All authors have read and agreed to the published version of the manuscript.

Funding: This research was funded by the Agencia Estatal de Investigación (AEI), project number PID2019–109517RB-I00 and the Xunta de Galicia ED431C 2022/18. ERDF funds are also acknowledged. This work was also financially supported by the Consellería de Cultura, Educación e Ordenación Universitaria of the Galician Government: EM2014/022 to A.C. M.A. thanks Xunta de Galicia and the ERDF (ED431C 2021/21).

Institutional Review Board Statement: Not applicable.

Informed Consent Statement: Not applicable.

Data Availability Statement: Data is contained within the article and supplementary material.

Acknowledgments: The authors are grateful for the work of the following technicians: Antonio L. Llamas-Saiz, X-ray Unit, Research Infrastructures Area, CACTUS Bldg., Campus Vida, University of Santiago de Compostela, E-15782 Santiago de Compostela, Spain. Raquel Antón Segurado, Unidade de Microscopía Electrónica e Confocal-RIAIDT, Edificio CACTUS, Campus Vida, USC. Estéban Guitián, Unidade de Espectrometría de Masas e Proteómica, Edificio CACTUS, Campus Vida, USC.

Conflicts of Interest: The authors declare no conflict of interest. The funders had no role in the design of the study; in the collection, analyses, or interpretation of data; in the writing of the manuscript; or in the decision to publish the results.

References

1. Bozkurt, Y.; Karayel, E. 3D printing technology; Methods, biomedical applications, future opportunities and trends. *J. Mater. Res. Technol.* **2021**, *14*, 1430–1450. [[CrossRef](#)]
2. Paul, G.M.; Rezaenia, A.; Wen, P.; Condoor, S.; Parkar, N.; King, W.; Korakianitis, T. Medical applications for 3D printing: Recent developments. *Mol. Med.* **2018**, *115*, 75.
3. Kitson, P.J.; Glatzel, S.; Chen, W.; Lin, C.G.; Song, Y.F.; Cronin, L. 3D printing of versatile reactionware for chemical synthesis. *Nat. Protoc.* **2016**, *11*, 920–936. [[CrossRef](#)] [[PubMed](#)]
4. Symes, M.D.; Kitson, P.J.; Yan, J.; Richmond, C.J.; Cooper, G.J.T.; Bowman, R.W.; Vilbrandt, T.; Cronin, L. Integrated 3D-printed reactionware for chemical synthesis and analysis. *Nat. Chem.* **2012**, *4*, 349–354. [[CrossRef](#)]
5. Kitson, P.J.; Marie, G.; Francoia, J.P.; Zalesskiy, S.S.; Sigerson, R.C.; Mathieson, J.S.; Cronin, L. Digitization of multistep organic synthesis in reactionware for on-demand pharmaceuticals. *Science* **2018**, *359*, 314–319. [[CrossRef](#)]
6. Bubliauskas, A.; Blair, D.J.; Powell-Davies, H.; Kitson, P.J.; Burke, M.D.; Cronin, L. Digitizing chemical synthesis in 3D printed reactionware. *Angew. Chem. Int. Ed.* **2022**, *61*, e202116108. [[CrossRef](#)]
7. Ludwig, T.; Boden, A.; Pipek, V. 3D printers as sociable technologies. *ACM Trans. Comput. Interact.* **2017**, *24*, 1–28. [[CrossRef](#)]
8. Noorani, R. *3D Printing: Technology, Applications, and Selection*, 1st ed.; CRC Press: Boca Raton, FL, USA, 2017; Chapter 1.
9. Climent, M.J.; Corma, A.; Iborra, S. Heterogeneous catalysts for the one-pot synthesis of chemicals and fine chemicals. *Chem. Rev.* **2011**, *111*, 1072–1133. [[CrossRef](#)]
10. Lucarelli, C.; Vaccari, A. Examples of heterogeneous catalytic processes for fine chemistry. *Green Chem.* **2011**, *13*, 1941–1949. [[CrossRef](#)]
11. Leadbeater, N.E.; Marco, M. Preparation of polymer-supported ligands and metal complexes for use in catalysis. *Chem. Rev.* **2002**, *102*, 3217–3274. [[CrossRef](#)]

12. Sun, Q.; Dai, Z.; Meng, X.; Xiao, F.S. Porous polymer catalysts with hierarchical structures. *Chem. Soc. Rev.* **2015**, *44*, 6018–6034. [[CrossRef](#)] [[PubMed](#)]
13. Wassel, A.R.; El-Naggar, M.E.; Shoueir, K. Recent advances in polymer/metal/metal oxide hybrid nanostructures for catalytic applications: A review. *J. Environ. Chem. Eng.* **2020**, *8*, 104175. [[CrossRef](#)]
14. Sarkar, S.; Guibal, E.; Quignard, F.; SenGupta, A.K. Polymer-supported metals and metal oxide nanoparticles: Synthesis, characterization, and applications. *J. Nanoparticle Res.* **2012**, *14*, 715. [[CrossRef](#)]
15. Meldal, M.; Diness, F. Recent fascinating aspects of the CuAAC click reaction. *Trends Chem.* **2020**, *2*, 569–584. [[CrossRef](#)]
16. Liu, J.; Liu, W.; Xu, M.; Wang, B.; Zhou, Z.; Wang, L. Sensitive detection of Au(III) using regenerative rhodamine B-functionalized chitosan nanoparticles. *Sens. Actuators B Chem.* **2016**, *233*, 361–368. [[CrossRef](#)]
17. McGlacken, G.P.; Fairiamb, I.J.S. Palladium-catalysed cross-coupling and related processes: Some interesting observations that have been exploited in synthetic chemistry. *Eur. J. Org. Chem.* **2009**, *2009*, 4011–4029. [[CrossRef](#)]
18. Saldan, I.; Semenyuk, Y.; Marchuk, I.; Reshetnyak, O. Chemical synthesis and application of palladium nanoparticles. *J. Mater. Sci.* **2015**, *50*, 2337–2354. [[CrossRef](#)]
19. Polshettiwar, V.; Len, C.; Fihri, A. Silica-supported palladium: Sustainable catalysts for cross-coupling reactions. *Coord. Chem. Rev.* **2009**, *21–22*, 2599–2626. [[CrossRef](#)]
20. Mikhaylov, V.N.; Sorokoumov, V.N.; Liakhov, D.M.; Tskhovrebov, A.G.; Balova, I.A. Polystyrene-Supported Acyclic Diaminocarbene Palladium Complexes in Sonogashira Cross-Coupling: Stability vs. Catalytic Activity. *Catalysts* **2018**, *8*, 141. [[CrossRef](#)]
21. Lu, J.; Dimroth, J.; Weck, M. Compartmentalization of incompatible catalytic transformations for tandem catalysis. *J. Am. Chem. Soc.* **2015**, *137*, 12984–12989. [[CrossRef](#)]
22. Park, S.H.; Kim, J.L.; Kang, M.K.; Gong, J.U.H.; Han, S.Y.; Shim, J.H.; Lim, S.S.; Kang, Y.H. Sage weed (*Salvia Plebeia*) extract antagonizes foam cell formation and promotes cholesterol efflux in murine macrophages. *Int. J. Mol. Med.* **2012**, *30*, 1105–1112. [[CrossRef](#)] [[PubMed](#)]
23. Matsunaga, S.; Shibasaki, M. Recent advances in cooperative bimetallic asymmetric catalysis: Dinuclear schiff base complexes. *Chem. Commun.* **2013**, *50*, 1044–1057. [[CrossRef](#)] [[PubMed](#)]
24. Zhang, L.; Sonaglia, L.; Stacey, J.; Lautens, M. Multicomponent multicatalyst reactions (MC)2R: One-pot synthesis of 3,4-dihydroquinolinones. *Org. Lett.* **2013**, *15*, 2128–2131. [[CrossRef](#)] [[PubMed](#)]
25. Peters, R.J.R.W.; Marguet, M.; Marais, S.; Fraaije, M.W.; van Hest, J.C.M.; Lecommandoux, S. Cascade reactions in multicompartmentalized polymersomes. *Angew. Chem. Int. Ed. Engl.* **2014**, *53*, 146–150. [[CrossRef](#)]
26. Qu, P.; Cleveland, J.W.; Ahmed, E.; Liu, F.; Dubrawski, S.; Jones, C.W.; Weck, M. Compartmentalisation of molecular catalysts for nonorthogonal tandem catalysis. *Chem. Soc. Rev.* **2022**, *51*, 57–70. [[CrossRef](#)]
27. Houghten, R.A. General method for the rapid solid-phase synthesis of large numbers of peptides: Specificity of antigen-antibody interaction at the level of individual amino acids. *Proc. Natl. Acad. Sci. USA* **1985**, *82*, 5131–5135. [[CrossRef](#)]
28. Phan, N.T.S.; Gill, C.S.; Nguyen, J.V.; Zhang, Z.J.; Jones, C.W. Expanding the utility of one-pot multistep reaction networks through compartmentation and recovery of the catalyst. *Angew. Chem. Int. Ed.* **2006**, *45*, 2209–2212. [[CrossRef](#)]
29. Cleveland, J.W.; Choi, J., II; Sekiya, R.S.; Cho, J.; Moon, H.J.; Jang, S.S.; Jones, C.W. Cooperativity in the aldol condensation using bifunctional mesoporous Silica-Poly(Styrene) MCM-41 organic/inorganic hybrid catalysts. *ACS Appl. Mater. Interfaces* **2022**, *14*, 11235–11247. [[CrossRef](#)]
30. Helms, B.; Guillaudeu, S.J.; Xie, Y.; McMurdo, M.; Hawker, C.J.; Fréchet, J.M.J. One-pot reaction cascades using star polymers with core-confined catalysts. *Angew. Chem. Int. Ed.* **2005**, *44*, 6384–6387. [[CrossRef](#)]
31. Diaz-Marta, A.S.; Tubío, C.R.; Carbajales, C.; Fernández, C.; Escalante, L.; Sotelo, E.; Guitián, F.; Barrio, V.L.; Gil, A.; Coelho, A. Three-dimensional printing in catalysis: Combining 3D heterogeneous copper and palladium catalysts for multicatalytic multicomponent reactions. *ACS Catal.* **2018**, *8*, 392–404. [[CrossRef](#)]
32. Ciriminna, R.; Carà, P.D.; Sciortino, M.; Pagliaro, M. Catalysis with doped sol-gel silicates. *Adv. Synth. Catal.* **2011**, *353*, 677–687. [[CrossRef](#)]
33. Cane, A.; Tournaire, M.C.; Barritault, D.; Crumeyrolle-Arias, M. The endogenous oxindoles 5-hydroxyoxindole and isatin are antiproliferative and proapoptotic. *Biochem. Biophys. Res. Commun.* **2000**, *276*, 379–384. [[CrossRef](#)] [[PubMed](#)]
34. Vine, K.L.; Locke, J.M.; Ranson, M.; Benkendorff, K.; Pyne, S.G.; Bremner, J.B. In vitro cytotoxicity evaluation of some substituted isatin derivatives. *Bioorg. Med. Chem.* **2007**, *15*, 931–938. [[CrossRef](#)] [[PubMed](#)]
35. Singh, G.S.; Singh, T.; Lakhan, R. Synthesis, C-13 NMR and anticonvulsant activity of new isatin-based spiroazetidinones. *Indian J. Chem.* **1997**, *36*, 951–954.
36. Verma, M.; Pandeya, S.N.; Singh, K.N.; Stables, J.P. Anticonvulsant activity of schiff bases of isatin derivatives. *Acta Pharm.* **2004**, *54*, 49–56. [[PubMed](#)]
37. Pandeya, S.N.; Yogeeshwari, P.; Sriram, D.; Nath, G. Synthesis, antibacterial and antifungal activities of N-Mannich bases of 3-(N²-Pyrimethaminylo) isatin. *Indian J. Pharm. Sci.* **2002**, *64*, 209–212.
38. Selvam, P.; Muruges, N.; Chandramohan, M.; Debyser, Z.; Witvrouw, M. Design, synthesis and AntiHIV activity of novel isatine-sulphonamides. *Indian J. Pharm. Sci.* **2008**, *70*, 779–782. [[CrossRef](#)]
39. Sridhar, S.K.; Ramesh, A. Synthesis and pharmacological activities of hydrazones, schiff and mannich bases of isatin derivatives. *Biol. Pharm. Bull.* **2001**, *24*, 1149–1152. [[CrossRef](#)]

40. Ferraz de Paiva, R.E.; Vieira, E.G.; Rodrigues da Silva, D.; Wegermann, C.A.; Costa Ferreira, A.M. Anticancer compounds based on isatin-derivatives: Strategies to ameliorate selectivity and efficiency. *Front. Mol. Biosci.* **2021**, *7*, 627272. [[CrossRef](#)]
41. Dhokne, P.; Sakla, A.P.; Shankaraiah, N. Structural insights of oxindole based kinase inhibitors as anticancer agents: Recent advances. *Eur. J. Med. Chem.* **2021**, *216*, 113334. [[CrossRef](#)]
42. Brandão, P.; Marques, C.S.; Carreiro, E.P.; Pineiro, M.; Burke, A.J. Engaging isatins in Multicomponent Reactions (MCRs)—Easy access to structural diversity. *Chem. Rec.* **2021**, *21*, 924–1037. [[CrossRef](#)] [[PubMed](#)]
43. Brandão, P.; Puerta, A.; Padrón, J.M.; Kuznetsov, M.L.; Burke, A.J.; Pineiro, M. Ugi adducts of isatin as promising antiproliferative agents with druglike properties. *Asian J. Org. Chem.* **2021**, *10*, 3434–3455. [[CrossRef](#)]
44. Kudo, M.; Cheng, A.L.; Park, J.W.; Park, J.H.; Liang, P.C.; Hidaka, H.; Izumi, N.; Heo, J.; Lee, Y.J.; Sheen, I.S.; et al. Orantinib versus placebo combined with transcatheter arterial chemoembolisation in patients with unresectable hepatocellular carcinoma (ORIENTAL): A randomised, double-blind, placebo-controlled, multicentre, phase 3 study. *Lancet Gastroenterol. Hepatol.* **2018**, *3*, 37–46. [[CrossRef](#)] [[PubMed](#)]
45. Chow, L.Q.M.; Eckhardt, S.G. Sunitinib: From rational design to clinical efficacy. *J. Clin. Oncol.* **2007**, *25*, 884–896. [[CrossRef](#)]
46. Roth, G.J.; Binder, R.; Colbatzky, F.; Dallinger, C.; Schlenker-Herceg, R.; Hilberg, F.; Wollin, S.L.; Kaiser, R. Nintedanib: From discovery to the clinic. *J. Med. Chem.* **2015**, *58*, 1053–1063. [[CrossRef](#)]
47. Han, K.; Zhou, Y.; Liu, F.; Guo, Q.; Wang, P.; Yang, Y.; Song, B.; Liu, W.; Yao, Q.; Teng, Y.; et al. Design, synthesis and in vitro cytotoxicity evaluation of 5-(2-Carboxyethenyl) isatin derivatives as anticancer agents. *Bioorg. Med. Chem. Lett.* **2014**, *24*, 591–594. [[CrossRef](#)]
48. Teng, Y.O.; Zhao, H.Y.; Wang, J.; Liu, H.; Le Gao, M.; Zhou, Y.; Han, K.L.; Fan, Z.C.; Zhang, Y.M.; Sun, H.; et al. Synthesis and anti-cancer activity evaluation of 5-(2-Carboxyethenyl)-isatin derivatives. *Eur. J. Med. Chem.* **2016**, *112*, 145–156. [[CrossRef](#)]
49. Chang, Y.; Yuan, Y.; Zhang, Q.; Rong, Y.; Yang, Y.; Chi, M.; Liu, Z.; Zhang, Y.; Yu, P.; Teng, Y. Effects of an isatin derivative on tumor cell migration and angiogenesis. *RSC Adv.* **2020**, *10*, 1191–1197. [[CrossRef](#)]
50. Firozpour, L.; Gao, L.; Moghimi, S.; Pasalar, P.; Davoodi, J.; Wang, M.W.; Rezaei, Z.; Dadgar, A.; Yahyavi, H.; Amanlou, M.; et al. Efficient synthesis, biological evaluation, and docking study of isatin based derivatives as caspase inhibitors. *J. Enzym. Inhib. Med. Chem.* **2020**, *35*, 1674–1684. [[CrossRef](#)]
51. Beletskaya, I.P.; Cheprakov, A.V. The heck reaction as a sharpening stone of palladium catalysis. *Chem. Rev.* **2000**, *100*, 3009–3066. [[CrossRef](#)]
52. Fouad, M.A.; Abdel-Hamid, H.; Ayoup, M.S. Two decades of recent advances of Ugi reactions: Synthetic and pharmaceutical applications. *RSC Adv.* **2020**, *10*, 42644–42681. [[CrossRef](#)]
53. Pal, R. Amberlyst-15 in organic synthesis. *Arch. Org. Chem.* **2015**, *2012*, 570–609.
54. Gautier, A. Ueber die einwirkung des chlorwasserstoffs u. a. auf das aethyl- und methylcyanür. *Justus Liebigs Ann. Chem.* **1867**, *142*, 289–294. [[CrossRef](#)]
55. Hofmann, A.W. Ueber eine neue reihe von homologen der cyanwasserstoffsäure. *Justus Liebigs Ann. Chem.* **1867**, *144*, 114–120. [[CrossRef](#)]
56. Azuaje, J.; Coelho, A.; El Maatougui, A.; Blanco, J.M.; Sotelo, E. Supported P-toluenesulfonic acid as a highly robust and eco-friendly isocyanide scavenger. *ACS Comb. Sci.* **2011**, *13*, 89–95. [[CrossRef](#)] [[PubMed](#)]
57. Sotelo-Perez, E.; Azuaje-Guerrero, J.A.; Coelho-Coton, A.J. Method for Capturing Isocyanides. WO2012049345A1, 19 April 2012.
58. Biswas, K.; Ghosh, S.; Basu, B. Ion-exchange resins and polypeptide supported catalysts: A critical review. *Curr. Green Chem.* **2020**, *7*, 40–52.
59. Silva, T.R.; de Oliveira, D.C.; Pal, T.; Domingos, J.B. The catalytic evaluation of bimetallic Pd-based nanocatalysts supported on ion exchange resin in nitro and alkyne reduction reactions. *New J. Chem.* **2019**, *43*, 7083–7092. [[CrossRef](#)]
60. Friedrich, K. *Structure and Properties of Additive Manufactured Polymer Components*; Woodhead Publishing: Cambridge, UK, 2020.
61. Maddah, H.A. Polypropylene as a promising plastic: A review. *Am. J. Polym. Sci.* **2016**, *6*, 1–11.
62. Available online: <https://www.hmcpolymers.com/storage/download/hmc-pp-chemical-resistance.pdf> (accessed on 9 February 2023).
63. Tri, N.M.; Thanh, N.D.; Ha, L.N.; Anh, D.T.T.; Toan, V.N.; Giang, N.T.K. Study on synthesis of some substituted N-Propargyl isatins by propargylation reaction of corresponding isatins using potassium carbonate as base under ultrasound- and microwave-assisted conditions. *Chem. Pap.* **2021**, *75*, 4793–4801. [[CrossRef](#)]
64. Alonso, F.; Moglie, Y.; Radivoy, G. Copper nanoparticles in click chemistry. *Acc. Chem. Res.* **2015**, *48*, 2516–2528. [[CrossRef](#)]
65. Koraneekit, A.; Limpaboon, T.; Sangka, A.; Boonsiri, P.; Daduang, S.; Daduang, J. Synergistic effects of cisplatin-caffeic acid induces apoptosis in human cervical cancer cells via the mitochondrial pathways. *Oncol. Lett.* **2018**, *15*, 7397–7402. [[CrossRef](#)] [[PubMed](#)]

66. Robledo-Cadena, D.X.; Gallardo-Pérez, J.C.; Dávila-Borja, V.; Pacheco-Velázquez, S.C.; Belmont-Díaz, J.A.; Ralph, S.J.; Blanco-Carpintero, B.A.; Moreno-Sánchez, R.; Rodríguez-Enríquez, S. Non-steroidal anti-inflammatory drugs increase cisplatin, paclitaxel, and doxorubicin efficacy against human cervix cancer cells. *Pharmaceuticals* **2020**, *13*, 463. [[CrossRef](#)] [[PubMed](#)]
67. Bayoumi, H.M.; Alkhatib, M.H.; Al-Seeni, M.N. Carvacrol effect on toptecan cytotoxicity in various human cancer cells in vitro. *Pharmacia* **2021**, *68*, 353–363. [[CrossRef](#)]

Disclaimer/Publisher’s Note: The statements, opinions and data contained in all publications are solely those of the individual author(s) and contributor(s) and not of MDPI and/or the editor(s). MDPI and/or the editor(s) disclaim responsibility for any injury to people or property resulting from any ideas, methods, instructions or products referred to in the content.